Surface Engineering of Cu-Catalysts for Electrochemically Reduction of CO_2 to Value-Added Multi-Carbon Products

Hassina Tabassum,[1,2+] Xiaoxuan Yang,[1+] Ruqiang Zou,[2]* and Gang Wu[1]*

[1]Department of Chemical and Biological Engineering, University at Buffalo, The State University of New York, Buffalo, New York 14260, United States.

E-mail: gangwu@buffalo.edu

[2]Beijing Key Lab of Theory and Technology for Advanced Battery Materials, Department of Materials Science and Engineering, College of Engineering, Peking University, Beijing, 100871, China.

E-mail: rzou@pku.edu.cn

+: These two authors contributed equally

SUMMARY

Copper (Cu) is the most efficient metal that can electrochemically convert CO_2 to various chemical feedstocks at reasonable efficiency. The activity and selectivity toward the CO_2 reduction reaction (CO_2RR) largely depend on the surface sensitivity and electrokinetics of Cu catalysts. Surface engineering is achievable through tuning the structure, and crystal orientation. The Cu-surface modulation and tunings, *e.g.*, controlled morphology, oxygen vacancies, and alloys on supports or substrates propose different reaction tracks and intermediates, while common routes are *CO dimerization, C-C, and C_1-C_2 coupling for the formation of C_2 and C_3 products. In this review, recent progress on the surface engineering of Cu-based catalysts is primarily recaptured and explained. The fragmentation, coalescence, and aggregation of Cu nanoparticles cause stability issues of Cu catalysts during the CO_2RR, which has also been discussed. Finally, we summarize

critical strategies and approaches to surface engineering of Cu-based catalysts for the efficient CO_2RR.

1. INTRODUCTION

Atmospheric carbon dioxide (CO_2) emission has increased by 2.2% per annum from fossil fuels and industry. Global emission needs to reduce and limit the climate change to below 2ºC warming, which is one of the plans of the Paris agreement among eighteen developed economies,[1] spotlighting the importance of carbon-neutral processes.[2-4] The efficient electroreduction of CO_2 into beneficial hydrocarbon fuels is an ultimate strategy to overcome the urgent need for renewable energy for the reduction of greenhouse gas emissions.[2,5-15] Large input energy is required for the activation of CO_2 because different reaction pathways are needed to result in multi-carbon products with high selectivity. Thus, an exceptional catalyst engineering inventory promotes these multiple processes for the CO_2 reduction reaction (CO_2RR) through direct electrical energy input under ambient conditions.[16-23] In particular, copper (Cu)-based materials have been explored widely for the CO_2RR to the valuable products of fuels and chemicals with decent efficiency. In contrast, Cu-free catalysts have also shown the property for the CO_2RR to C_{2+} products but low faradaic efficiency (FE) limits further use. Cu has the negative adsorption energy for *CO, which serves as an essential intermediate in CO_2RR, and reaches a balance between *CO_2 and hydrogenation of *CO to proceeding hydrocarbon products, bestowing Cu with unique properties to find product beyond CO. However, this faces greater challenges for an ideal Cu-based catalyst toward a specific product. Polycrystalline copper foil for the CO_2RR, for example, could produce more than sixteen various products which require energy-intensive separations,[24,25] highlighting the CO_2RR dependence and sensitivity to the surface of Cu catalysts. The sensitivity to the Cu-surface pointed to the surface reconstruction or evolution of Cu catalysts under CO_2RR, which results in the modified electronic structure, surface oxidation states, and atomic arrangements,[25-28] thus having dominant impacts on the catalytic performance (discussed in Section 3).[29-31] Although the chemical

and structural states of Cu-surface in CO_2RR are still under debate and remain elusive, surface engineering is crucial to enhance the selectivity and activity for the CO_2RR to particular hydrocarbon. The pioneering work on surface engineering of catalysts for the CO_2RR was reported by Hori *et al*. in 1985, which predicted that product selectivity is related to the facets of Cu single crystal, such as selective CO_2 reduction to ethylene and methane on Cu(100) and Cu(111), respectively.[32-34] To date, several studies have focused on the alteration in the surface structure of Cu catalysts to enhance their FE towards energy-dense products.[35,36] While many detailed reviews and prospective articles have been published on Cu and non-Cu catalysts for the CO_2RR, a focused surface engineering of Cu catalysts would be highly demanded to provide a unique insight into how to rationally design highly active and selective catalysts for the CO_2RR.[32,37,38] Besides these extensive studies, there is still a need to elaborate the concept of Cu-surface engineering because the Cu-surface can give the promising activity for the CO_2RR to C_{2+} products to neutralize the carbon in the environment.

Herein, we aim to provide a comprehensive review of surface engineering Cu catalysts for the CO_2RR to tune its selectivity and catalytic activity. We also discuss how the optimized surface, phase effects, morphology, and structure of catalyst influence the catalytic performance and reasons of Cu-catalysts' instability during CO_2RR.

2. MECHANISTIC VIEW OF THE CO_2RR AT CU SURFACE

Cu has been widely applied for the CO_2RR because of its inherent properties to produce multi-carbon products at modest overpotentials.[39-50] The different Cu-surface would affect the structure of adsorbates, leading to the generation of different intermediates and reaction tracks during the structure-sensitive CO_2RR process. Therefore, it is compulsory to sufficiently understand the reaction routes on Cu-surface to hydrocarbons.

The electroreduction of CO_2 on the surface of Cu proceeds multiple electron-proton transfers and generates multiple intermediates through several pathways, producing a range of products simultaneously. The Cu-surface is the only surface to generate at least 16 hydrocarbon products because of adequate *CO adsorption and nominate the complexity of the mechanism. As simplified, the adsorbed *CO with the assistance of one electron and one proton (*H) on the Cu-surface produces intermediates (*COH or *CHO), and forms *OCCO *via* the C−C bond coupling. Further combination of *COH and *CO produces *COCOH, and then undergoes a series of multiple proton-coupled electron transfer (PCET) processes to yield various C_{2+} products, which could be tuned and directed by surface engineering of Cu-catalysts for the CO_2RR through atomic arrangements, geometry, and Cu-facets for particular hydrocarbon products.[25,51-53] Therefore, a deep understanding of the mechanistic view of CO_2RR is required for surface engineering of efficient electrocatalysts to control the reaction steps and obtain desired products. Jaramillo's group has drawn a flow for the consensus, and summarized the reaction tracks of three decades working for the CO_2RR on Cu-surface with different tuned structures (**Figure 1**).[32] As described, the early theoretical studies presented the primary C-C mechanism and multi-electron transfer reactions, and explored diverse C_2 products combined with experimental observations. Furthermore, the dimerization of *CO is a common concept for producing the >2e$^-$ products (*e.g.*, C_2H_4, C_2H_5OH, and n-C_3H_7OH) on bulk Cu-surfaces. Details of these complicated tracks can be found elsewhere.[32,54-57] For a typical reduction of CO_2 to C_2H_4, the surface structure of single-crystal Cu-catalyst presented promoted *CO dimerization and higher C_2H_4 selectivity on Cu(100) than Cu(111), which further indicated the effect of surface engineering on the products.[32]

Qiao *et al*. also presented a road map on the Cu-surface for the CO_2RR to the formation of different C_2 products such as CH_3COOH, $C_2H_2O_2$ (< 1%), $C_2H_6O_2$, and C_2H_6 produced by utilizing

*CHO and *COH intermediates, respectively.[58] Experimental protocols also validate these complicated pathways of C_2 products. During CO_2 reduction to C_2, the CH_3 is a key intermediate, in which C_2H_6 has been produced through the dimerization of $*CH_3$, which were also empirically confirmed through isotopic studies on oxide derived Cu-surface.[59,60] The *CHO is a precursor for the formation of CH_4, which also promotes the formation of $C_2H_4O_2$ and $C_2H_6O_2$ through the CO inclusion mechanism. Conclusively, the most accepted agreement of C_2 formation is the *CO dimerization, and the C-C coupling on Cu(100) is the primary stage of the rate-determining step for a complete track for C_2-products.[61-63] Additionally, theoretical studies evidence that strong binding of CO-CO-, $*CH_2CHO$ converts to $*CH_3CHO$ and $*CH_3CH_2O$.[39,64,65] Besides, for more complicated C_3 products, the key protocol of *CO-CO for higher FE could be realized on the designed Cu-cavity type morphology with a modified electronic structure, in which the structure of Cu NPs with nanocavities effectively concentrates C_2 species, and promotes the formation of C_3 products *via* the confinement of C_2 intermediates.[66] However, few *in-situ* spectroscopy studies support that C_2 intermediates (*e.g.*, $(*CH_3CH)$-CH_2CHO or $*CH_3$-CH)) could couple with adjacent C_1 products to form CH_3CH_2CHO, therefore, C_3-pathway is still unresolved.[65] Overall, based on the literature survey, we found that different engineered Cu-surface, and morphologies followed different intermediate routes for the CO_2RR, while common routes are *CO dimerization, C-C and C_1-C_2 coupling for the formation of C_2 and C_3 products. The particular type of products could be obtained through CO_2RR on specific controlled engineered Cu-surface.

3. SURFACE ENGINEERING OF CU-BASED ELECTROCATALYSTS

Surface engineering is an effective strategy for tuning surface structure by the insertion of foreign metal or non-metal elements into Cu-structure with controlled facets, shapes and oxidation states to stabilize the catalyst surface for the CO_2RR. Surface engineering of Cu-based electrocatalysts

plays a vital role in improving activity and selectivity. The surface can be tuned and engineered through various applied protocols to reconstruct electrocatalysts.[67-69] There are several ways to alternate surface modulation and tunings, such as morphology control, the inclusion of oxygen vacancies, and the insertion of secondary transition metal species to form Cu alloys on supports or substrates. Recently, for example, surface roughness or specific modified structure of the Cu-based electrode has proven to be effective for enhancing activity/selectivity in CO_2RR.[70] Furthermore, the tuned electronic structure, chemical composition, atomic arrangements, and surface oxidation states promote the CO_2RR process.[30] The brief overview of these properties has given below.

The electronic effect. The tunable composition in Cu-based alloys (*i.e.*, Cu-Au) has been correlated with the variation in electronic properties.[71-74] The d-band center moves away from the Fermi level because of the higher atomic ratio of foreign elements (*i.e.*, Au), and modifies the electronic structure, resulting in optimized binding energy for *CO and *COOH intermediates to promote activity and selectivity of CO_2RR.[31,75-78] Experimentally, electrochemical impedance spectroscopy (EIS) and powder X-ray diffraction (PXRD) characterize the possible coinciding between grain size, microstrain, and charge transfer resistance to know about the reactivity of catalysts. The lattice strain on the catalyst surface could affect the binding strength of intermediates and charge transfer resistance. For instance, the high microstrain presents low charge transfer resistance, and promotes the electrokinetics of catalysts. This particular correlation between charge transfer resistance and microstrain highlights the significance of electronic properties for the adsorption of reactant molecules and kinetics during CO_2RR. However, there is still a lack of clear vision about the decoupling of electronic structure, composition, and geometry.

Atomic arrangements. The Cu-surface has exhibited dynamic changes in chemical states under the applied potential and local environment. Engineering the atomic arrangement in Cu-alloys such as

sub-ordered structure, core-shell, and separated phase provides unique coordination numbers to control electron transfer steps and product selectivity.[25,79] Similarly, the two-dimensional surface of Cu foil possesses a polycrystalline structure. Polished polycrystalline foil with a primary facet of (111) can catalyze the C-C coupling for C_{2+} products with lowered efficiency for C_1 products. However, the Cu single crystal with (100) facet has been suggested more suitable for C_{2+} products than the (111) facet. It is worth noting that the support or substrate is also essential for depositing Cu species to create a novel interface for promoting the catalytic activity of CO_2RR. Therefore, it is of prime significance to preciously identify and select proper substrates to grow specific crystals and particular facet with desired products for the CO_2RR. A well-known example of Cu-deposition is a thin Cu film rich with active sites which conveyed high CO_2RR activity. The active surface can be engineered through epitaxial growth with several facets such as Cu(100), Cu(111), and Cu(751). In this context, the powerful *in-situ* electrochemical scanning tunneling microscopy (STM) could find evidence of the linking of lattices on the surface different from the bulk structure, further confirming that Cu(100) and Cu(751) facets are highly active for the CO_2RR. For example, the single crystal of Cu with the (100) facet provides a sensitive surface, which promotes the CO reduction to higher C-C coupling selectivity and activity for hydrocarbon production.[80] Besides, the presence of oxygen vacancies deposited on the Cu surface also facilitates the C-C coupling, thus exhibiting promising performance during CO_2RR with the faradaic efficiency (FE) for the ethylene and ethanol of ~45% and ~22%, respectively.[30,81]

Surface Oxidation States. The reconstruction of Cu-surface by oxidation has a great impact on the activity and selectivity of CO_2RR.[82] The controlled surface oxidation and adsorption of intermediates in CO_2RR are important for producing unique catalysts with selective products.[83] Experimentally, *in-situ* spectroscopies such as surface-enhanced infrared absorption spectroscopy

observed the adsorption states of CO on oxide-derived Cu catalysts for C_1 and C_{2+} products.[84] The developed grain boundaries on the as-prepared Cu electrode provide unique surface sites with low coordination, serving as the active sites for the CO_2RR. Among all the studied oxide-derived Cu catalysts, only Cu(I) sites could not improve the CO_2RR. However, the efficiency and selectivity could be significantly enhanced by incorporating Cu(I) and Cu(0) to induce a synergy, which enhanced the kinetics and thermodynamics of both CO_2 activation and CO dimerization for C_2 production.[32,83] Besides, the combination of the controlled morphology and oxides (*e.g.*, Cu_xO or CuO) or phases (*e.g.*, (111), (100), *etc*.) could tailor the active sites and enhance the surface area, thus increasing the CO_2RR performance for C_2 products. According to Wulff-constructed clusters, for example, Cu(100) phase presents a vital role in the electroreduction of CO_2 to C_2 product because of the reduced surface energy and enhanced stability of the intermediates than Cu(111).[81]

Surface engineering *via* the insertion of non-metal elements (S, N, Se, or P) into Cu structure enhances the active sites for CO dimerization during CO_2RR. The inclusion of S or Se species on the surface of the Cu electrode also produces C_2 product. In a similar context, the insertion of heteroatoms (N, S, or P) into carbon structure tuned the electronic spin, providing active sites for the CO_2RR. The pyridinic-N and pyrrolic-N moieties in carbon structure bestow unique catalytic activity for the CO_2RR.[78] The possible reduction mechanism occurs on the pyridinic-N when N is replaced into a C6 ring of graphitic structure, leaving a lone electron-pair at 120° from two N-C bonds and perpendicular to π-network. In contrast, the p-electrons of graphitic-N and pyrrolic-N were fully conjugated to graphitic π-network without any localized electron pairs. Consequently, the pyridinic-N dopant acts as a Lewis base for protonic bonding and interaction of CO_2 on the catalyst for reduction.

The Cu-surface can be modified through different controlled morphologies with a particular phase, metal or non-metal species insertion into the Cu surface in ordered or disordered ways, which presented different surface chemistry, surface reactions, and different selectivity of CO_2RR, as shown in **Figure 2**. Moreover, the active surface can be generated through Cu-vacancy, surface strains, and defects, enhancing the surface energy to promote the CO_2RR process. In this section, the most repetitive literature examples have been selected based on the perspectives of bulk Cu (polycrystalline Cu-surface, and Cu-foil), Cu-nanoparticles with different edges and shapes with particular face, non-metallic elements doped Cu-structures, and Cu-single atoms into nitrogen-doped carbon. The chemisorption of CO_2 with H_2O on Cu and physisorption of CO_2 with O on Cu-surface were discussed. Afterward, a brief discussion has given on stability issues with Cu-catalysts and techno-economic analysis for CO_2RR-electrolyser. Lastly, challenges and future perspectives were summarized.

3.1 Tuning Cu Surface for the CO_2RR

As mentioned above, CO_2RR is a complex process because of the multi-electron transfer steps on sensitive surface of Cu-catalysts.[85] Sensitive surface could relate to surface-reconstruction or structural evolution on primary Cu-surface under applied environment such as applied potential, plasma impulse and pH values in CO_2RR. Many reports have demonstrated tuned Cu-surface by controlling facet, crystal structure, morphology and valency could enhance the C-C coupling, which is a possible pathway for forming C_{2+} products on Cu-surface (*i.e.*, Cu(100)) with the catalytic role of existing oxygen and $Cu^{\delta+}$. In this regard, the existence of Cu(I) and Cu^0 on the catalytic surface was found to promote CO dimerization.[83,85-89] Nonetheless, Cu(I) was not stable under operando CO_2RR conditions. However, it could be stabilized with modifier elements or control over the exposed facets of traditional CuO-based catalysts to form the polycrystalline

surface. To better understand the control over CO_2RR selectivity, a well-defined active surface with known composition is quite compulsory. For instance, Rosa *et al*. presented a simultaneous effect on well-defined structure with Cu(I) species for the CO_2RR to multi-carbon products.[90] In particular, the anodic pulse was applied to the electrode at a particular defined potential, which facilitates the formation of oxidized Cu(100) surface with particular defects and coexistence of Cu^0 and Cu(I) species for selective products, thereby contributing to C_2 production. Similarly, the surface modification could be performed through cyclic voltammograms (CVs) on different single crystal electrodes in different pH of electrolytes.[87,91] A particular voltage could be selected for finding Cu's favored C-C coupling surface (100), for example, Cu_2O was formed at 0.3 V (vs. RHE), and CuO was presumed at 0.8 V (vs. RHE).[85,88] Moreover, the pretreatment process is essential for tuning or reconstructing the surface under CO_2RR. The surface morphology in different early treated samples with flat surfaces was transmuted to the granular surface under applied potentiostatic conditions (**Figure 3a-b**).[90] It is worth noting that the pulse time is necessary to tune the surface structure and composition. The Cu-surface could be changed by applying pulse in different exposure times, which can be also confirmed by using *in-situ* X-ray photoelectron spectroscopy (XPS) at different applied potentials. After continuous oxidation/reduction of the Cu-surface under positive applied potentials, large structures of the cubic island with facet (100) and step edge defects on their endings reduced to faint cubic structure because of surface defects (**Figure 3c-f**).[90] The same pulse conditions could be applied for the CO_2RR to monitor the surface alteration on Cu(100) and achieve higher selectivity of C_{2+} at 0.6 V. Similarly, final products of CO, CH_4, and C_2H_4 could be observed on the Cu surface at -1.0 V, and ethanol production with suppressed hydrogen evolution reaction (HER) on Cu(100) at 0.8 V. To summarize, the engineering Cu-surface with highly defective surface, well-ordered domains, roughness, and (100)

terraces produced synergy for the CO_2RR. Besides, the enhanced CO_2RR performance is also linked to the reproduction of Cu_2O. The pulsed electrolysis at a voltage of 0.6 V modified the well-defined domains (100) represented by the red color curve (**Figure 3g**). *In-situ* surface-reformation of Cu(I) also exhibited a noticeable impact for selectivity of C_{2+} products with reduced by 37% in the defective Cu(100) electrode without pulsed. Similar results were obtained under different cathodic pulse times, as shown in **Figure 3h**. Even in the presence of defects on the Cu(100) surface at a constant applied potential, C_1 products and HER process could occur in the absence of Cu(I) species. Thus, in addition to high oxophilicity Cu surface and Cu^0 under applied potential, the reconstruction surface with Cu(I) plays a significant role in inhibiting the HER for ethanol formation. Conclusively, the simultaneous existence of (100) domains, large defect sites, and Cu_2O surface is considered the most favorable for the CO_2RR to C_{2+} products. For ethanol selectivity, the Cu surface could be engineered for Cu(I) and Cu(0), whereas ethylene selectivity is dominant on the Cu(100) terraces. Thus, tuned surface structure and controlled composition could lead to higher production of the selective C_{2+} products.

Additionally, selective oxygen plasma is a scalable and controllable technique, which can also reconstruct and activate the Cu surface for the CO_2RR through changing the chemical states of Cu at ambient conditions and producing surface defects without sintering of NPs. Mistry *et al*. applied oxygen and hydrogen-based plasma to fabricate the novel oxide layers, porous surface structure, and tuned chemical states of polycrystalline Cu.[91] Besides, CuO is grew on the grain boundaries, such as microwires on a rough surface. Specific techniques of operando XPS and STEM could be carried out to find insights into the Cu^+ species and oxidative Cu surface for the CO_2RR. The plasma-activated surface of Cu was significantly reduced with enhanced porosity during CO_2RR, and more differences before and after CO_2RR were exhibited in STEM elemental

mapping (**Figure 4a-h**).[91] A transparent oxide layer was observed over metallic Cu film after the oxygen plasma treatment with a particular ratio of Cu : O (2.7 : 1.0) for the inner layer of Cu_2O and 1.3 : 1.0 for the upper layer of CuO. It is worth noting that at grain boundaries and structural domain, oxide growth is the fastest under oxygen plasma treatment. The single-layer consisting of 3 to 29% of oxygen atoms was observed where CuO was found over the layer, and rich Cu^+ sites remained stable during the reaction. The HRTEM images presented the the structure of Cu_2O inner layer/CuO outer layer converted to Cu-rich region after the reaction, which reduced the onset potential for the CO_2RR with FE of 60% at a particular voltage (-0.9 V vs. RHE). In contrast, the H_2 plasma-treated sample with the reduced active sites showed the worse activity for C_2H_4 products.

As another example, the surface of Cu gauze can also be modified through the surface growth of nanowires and coating with a microporous layer to form a gas diffusion electrode (GDE). After oxidation, the surface of the Cu gauze was covered by Cu_xO or $Cu(OH)_2$ (**Figure 4i-l**).[92] After additional coating with conducting carbon and polytetrafluoroethylene (PTFE), the Cu gauze was converted to a flat microporous layer and then cracked under heating (**Figure 4m-p**).[92] As a result, various morphologies and/or compositions resulted in the differentiate CO_2 electroreduction performance. For example, the CO_2RR on Cu nanowires derived from wet chemical oxidation (WCO-Cu) produced C_1. In contrast, upon thermally annealing, the Cu gauze (TA-Cu) produced C_2 products with an FE of 40% at current densities of 200 mA/cm^2 in a flow cell.

Furthermore, electrodeposition of the foam allows the interlinkage between Cu pores (**Figure 4q-v**),[93] where eventually, the color of the foam was altered to reddish, as shown in the inset of **Figure 4q**.[93] The dendrites structure protrudes on the edges of the pores of a specific diameter (20-50 μm) under controlled parameters of pH and deposition time, which exhibited 29% of HCOOH

production under ambient conditions.[93] Besides, Cu nanofoam presented the novel electrode structure for the CO_2RR, which depends on systematic changes including pore diameter, pore depth, and pH environment. The nanoporous Cu foam, for example, was prone to oxidation (CuO and Cu_2O) because of its higher surface area. After 30 s and 60 s of electrodeposition, the nanofoam of Cu formed the interconnected pore structure, and increased in thickness with extending electrodeposition time (**Figure 4w-x**).[94]

Besides experimental evidences, theoretical computations with density functional theory (DFT) and machine learning (ML) could determine the CO adsorption properties and constructive active sites visualization on Cu-surface for CO_2RR processes. The surface structural criteria could be optimized by calculating the reaction energies for intermediates and rate determine steps. The coupling study of ML for conceptually visualizing of reactive force field (ReaxFF-ML) for the large number of atoms (*e.g.*, 20,000) and DFT for calculating the reaction energies of intermediates could be a good methodology for advanced studies on Cu-surface engineering. Bell *et al*. presented the role of surface roughness for producing the higher selectivity for C_{2+} products and CO binding active sites on the Cu roughed surface by oxygenate to hydrocarbons. The ReaxFF-ML approach has predicted the CO-binding energy on the electrochemically polished and plasma treated Cu-surface to determine the low redox sites on particular Cu facets (*i.e.*, (111), (100) and (211)) (**Figure5a-c**).[95] The higher binding sites for CO were appeared on Cu(211) after plasma irradiation (**Figure 5c**) which are consistent to experimental for low selectivity of CO. The strong adsorption of CO* and H* on the Cu-surface is expected to the formation of hydrocarbon products. Similarly, Goddard *et al*. proposed the specific neural network model by using ReaxFF to find the adsorption energies over the wide range of surface sites, presented in a statistical view **(Figure 5d-e**).[96] There are different CO-adsorption energies (-0.55 to -1.43 eV) on the surface of Cu nanoparticles. The

Cu clusters presented the (111), (100) and (211) facets which evidenced the large number of active sites. Furthermore, ReaxFF-ML was also applied for interlacing the quantitative structural properties and CO-adsorption energies to indicate the active sites on different Cu-facets to improve the selectivity for hydrocarbon products The use of ML is suitable for predicting the CO-adsorption energy, surface structure and activity relationship, perfect extrapolation of experimental study, and selective active sites for the CO_2RR.

3.2 Tuned Shape of Cu Surface for the CO_2RR

Engineering Cu-surface with different edges, shapes, facet and oxidation states could control the reaction paths for the CO_2RR to particular hydrocarbon products. However, understanding the origin of activity and selectivity on the surface of Cu electrocatalysts is a challenging step. Initially, polycrystalline Cu foil was directly applied to convert CO_2 to hydrocarbons because of the metastable grain boundaries. Later, it was found that CO_2RR catalytic activity also depends on the morphology of the electrocatalysts. For example, Cu NPs could further enhance the superior catalytic activity for the CO_2RR than polycrystalline Cu foil due to their homogenous morphology with leading edges, high surface to volume ratio, and new exposed active sites.[97-105] The high surface energy facets on the modified Cu-surface have been regarded as a necessary part of a structure with high catalytic activity, stability and selectivity. In addition to the surface energy, the catalyst would become more active when the particle size was reduced to 50 nm due to uncoordinated sites on the surface, which tuned the electronic structure and enhanced the catalytic activity. Also, a smaller size introduced a significant strain of the surface atom, influencing the catalytic activity. Correspondingly, these catalyst properties can enhance the activity of the $2e^-$ processes, and promote intermediate rate-determining steps.[106,107] However, CO_2RR consists of

>2e$^-$ products, involving quite complex proton-electron transfers. Therefore, it is difficult to predict how tuning the electronic structure might affect the CO_2RR performance.

After reviewing several reported Cu-based electrocatalysts for the CO_2RR, we found that the product selectivity is directly related to Cu surface structure. For example, the ethylene, methane, ethanol were produced on Cu(100), Cu(111), and Cu(110), respectively.[40,58,83,108-114] Some reports claimed that the selectivity of ethylene could be greatly enhanced on the surface of Cu cubes of 100 nm with facets of (100) as well as a single crystal surface of (100). Besides, the size and shape of the catalysts also affected the selectivity and reaction tracks of CO_2RR. Usually, a well-known colloidal chemistry method was adopted for the controlled shapes of Cu spheres (7.5 to 27 nm) (**Figure 6a**).[115] Comparatively, the cubic shape of the Cu crystal presented more actively, for instance, about 80% carbon products involving 50% ethylene could be generated on the Cu cubes of 44 nm.[115] Besides, Suen *et al*. fabricated several Cu-shapes such as cubic (C-Cu), hexarhombic docadehedron (H-Cu), and octahedron (O-Cu) for the CO_2RR (**Figure 6b-c**).[116] Each Cu-shape is responsible for different products under CO_2RR. In particular, C-Cu could enhance the formation of ethylene, H-Cu is responsible for ethanol formation (~25%), and O-Cu could produce a large amount of CO and methane, which also revealed that the atomic arrangement on the Cu surface is essential for the selectivity of the various products. Moreover, the edges are also important for the attributed products because of high adsorption energy for *CO.[23,84] Different shapes consist of different edges, such as 6 Cu(100) planes with 12 edges for C-Cu and 4 Cu (100), 8 Cu(111) with 28 edges for H-Cu, and 8 Cu(111) planes with 12 edges for O-Cu. Another example of the oxide-derived Cu (OD-Cu) was found for the CO_2RR with higher activity for selectivity of C_{2+} products because of the rapid C-C coupling formation (**Figure 6d**).[110] In particular, Cu_2O NPs can also be synthesized with controllable facets for controlled CO_2RR catalytic activity. Particular facets of

Cu_2O can be controlled by using particular surfactants of hydroxylamine hydrochloride with additional surfactant (**Figure 6e**).[77] Besides, different facets and atomic arrangements on the Cu surface of porous Cu (P-Cu) microsphere with particular coordination number (CN) also presented good catalytic activity for C_{2+} products. For the CO_2RR, CN of 6 and 8 are promising for the CO=CO dimerization on the Cu surface. The effective methods to create surface energies include etching process and capping effects, which can convert the low-energy surface to a high-energy surface, and tune the surface energies during the formation of the crystals, respectively. For example, the cubic shape and the Cu crystal of the facet (110) often present high-energy facets for enhancing the CO_2RR. The work function value is also important to know about surface energy. Among the Cu facets of (100), (111), and (110), the (110) presents the smallest value of work function and the highest energy on the surface, which would be easier to be oxidized to promote the surface reactions. Similarly, dodecahedrons present a high surface energy (110) facet, which was produced *via* the etching process. With different etching duration, the shape of the particles was changed from (100) into (110) facets with higher surface energy (**Figure 6e**).[77] Etching processes longer than 12 h would only reduce the particle size rather than altering their shape fully enclosed by (110) facets. Furthermore, the adsorption of iodide ions on the surface of the compact Cu is responsible for the porous structure, which possesses moderate CN responsible for 78% selectivity of C_{2+} products (**Figure 6f-i**).[117] However, it is suspected that NPs of defined morphologies can interact during catalytic reactions but wherein they agglomerate to form larger-sized NPs with faded catalytic activity.

Besides, Cu-surface could be engineered by functionality with hydroxy groups (HCO_3^-, and OH^-), promoting the selectivity for the CO_2RR and suppressing the HER. For a $Cu_2O(111)$ octahedral catalyst, for example, the hydroxy groups on Cu-surface tuned the charge transfer

mechanism, mass transport, and enhanced the adsorption energy of *COOH.[76] Furthermore, the cationic homopolymers and tricomponent copolymer on Cu-surface influenced the activity and selectivity for the CO_2RR, which improves the access of reactants and reduces the blockage of active sites on surface.[118-120]

3.3 Engineering of Cu Surface through the Insertion of Metallic Species

While the surface engineering and structural evolution could regulate the activity and selectivity of particular electrochemical processes, several scientists have also tried to mix other metals with Cu to produce a strong synergy for the CO_2RR with high FE values for C_{2+} products. As a result, bimetallic Cu-based catalysts, such as CuAu, CuPd, CuZn, CuFe, and CuSn catalysts have been reported widely. Benefiting from different atomic arrangements, tuned binding energy, enhanced reaction kinetics, and modified reaction pathways for the CO_2RR, bimetallic catalysts usually present high selectivity for hydrocarbons production.[50,119,121-126] For the synthesis of bimetallic catalysts, the accurate regulation of composition or bimetal ratio, and the rational modulation of structures and morphologies[49,127] are of prime significance to enhance the catalytic performance. Generally, chemical reactivity of two different metals can merge and produce a unique bimetallic configuration with advanced properties. For example, Cu and Sn can be combined in three different structures, *i.e.*, CuSn NPs/C-A heterostructure, CuSn NPs/C-H with core-shell structure, and CuSn NPs/C-AH with Janus structure under various controlled conditions of annealing and pre-treatment (**Figure 7a-b**),[128] conveying different activities of CO_2RR. The TEM and HAADF-STEM images presented that CuSn NPs are dispersed with a diameter of 23 nm. The composition of CuSn consisted of 80.7/19.3 (Cu/Sn), which can be confirmed by energy-dispersive X-ray spectroscopy. The Cu phase was cubic (fcc) with an amorphous structure of Sn. The existence of $3d_{5/2}$ and $3d_{3/2}$ in CuSn corresponds to Sn^{4+} with SnO_2, found as a shell with a thickness of 1.48

nm. Both Cu and Sn are active elements for the CO_2RR in 0.1 M $KHCO_3$, producing primary CH_4 and C_2H_4 at -1.0 and -1.1 V, respectively. The interface of Cu/SnO_2 could also affect the CO_2RR activity on the heterostructure of Cu-SnO_2. Theoretical studies correlate to a Sn_6O_{12} cluster bounded on the Cu(111) slab to further elucidate the Cu/SnO_2 interfaces effect (**Figure 7c**).[128] The O atom contributed for hydrogenation on the surface of Cu/SnO_2, yielding *COOH species at 0.52 eV. The formation of *COOH intermediates is more favorable than that of OCHO* with ΔG of 0.85 eV, thus promoting the removal of H_2O, and activating the *CO with ΔG of -0.13 eV to form CO. Besides, the reactive site of SnO_2 promotes higher efficiencies for H_2 and HCOOH amounts. Benefitting from the abundant Cu/SnO_2 interfaces in the Cu-Sn heterostructure, as a result, CuSn NPs/C-A presented the best CO_2RR performance with FE of 70% from CO to HCOOH, as well as the long-term stability at -0.7 V, which further highlighted the importance of surface engineering Cu through additional metal atoms insertions along with the accurately structural regulation.[128] Similarly, Cu_2O-SnO_2 based cubic crystal with core-shell morphology also produced as trace yield of C and C_{2+} products at the cathodic potential of < -0.8 V. This activity was related to Cu and Sn active sites which can be tuned by relevant compositional ratio.[51,129-131]

Furthermore, noble metals such as Ag, Pd, and Au also exhibit high efficiency of CO, can be bound to Cu as a bimetallic catalyst, or a tandem catalyst. In an example of the Au island on Cu catalysts (Au-i@Cu), DFT calculations predicted the high catalytic activity due to the creation of a bimetallic interface instead of alloy.[132] Besides, the segregated phase of Cu/Pd electrocatalysts presented the encouraging performance for ethylene production.[133] Therefore, constructing the interface of heterojunction among bimetallic catalysts played an role in efficient CO_2RR. Furthermore, Ag is a conductive element that enhances the CO production among hydrocarbons,[110] thus inspiring the creation and development of Ag/Cu heterojunction where CO is produced in the

first step and then reduced on the adjacent Cu atoms to hydrocarbons. For example, the dispersion of tiny Ag NPs on Cu-surface produced heterojunctions responsible for the excellent activity of CO_2RR.[134] The EDS mapping of Ag/Cu catalysts exhibited the small Ag distributed and embedded over Cu (**Figure 7d-e**). The GC and NMR spectrometer determines the CO, C_2H_5OH, C_2H_4, and HCOOH composition in the products (**Figure 7f-g**). Comparatively, Ag/Cu is considered suitable for C_2H_4 with an FE of 42% at -1.1 V. Besides, different reported activity and selectivity of Cu-based electrocatalysts in the various mediums have been summarized in **Table 1**.

In another example, Cu nanowires with a homogenous dispersed thin layer of indium (In) were observed in the STEM elemental mapping images (**Figure 7h-j**).[135] The Cu and In consisted of the diffraction faces of (111) and (101), respectively. The In existed on the Cu nanowires and provided a particular interface of Cu-In, which enhances CO of FE 90% and stability for 60 h at a low potential value with an intermediate of *COOH. Moreover, formic acid (HCOOH) also emerged on the CuIn surface at -0.8 V and at -1.0 V, respectively.[135] Furthermore, the $In(OH)_3$ decorated on Cu presented a prominent role for the highest CO selectivity, and the Cu-In alloy was highly active and stable. These controlled interfaces elucidate the large active sites and synergistic effect of the metallic phases.[136] For producing more interfaces, hydroxides of Zn, Cd, Sb, and Pb were deposited on hydroxides of Cu foam, respectively.[137] Among different interfaces of CdCu@Cu, ZnCu@Cu, PbCu@Cu, and SbCu@Cu, CdCu@Cu presented the highest selectivity for the production of formate with 70.5% FE at a current density of -30.5 mA cm^{-2}. In contrast, ZnCu@Cu, PbCu@Cu showed moderate performance in forming formate. Thus, these interfaces provide guidelines for Cu-alloy surface modifications towards CO_2RR to high-value-added multicarbon products.

3.4 Engineering Cu Surface Through the Insertion of Non-metallic and Metalloid Elements

As summarized thus far, surface engineering of Cu-electrocatalysts for the CO_2RR to hydrocarbons have been studied broadly and multi-carbon products with high energy densities are in demand.[138] For example, the Cu-surface structure can be tuned for desired alcohol products with suppressed alkane and alkene formation. Understanding the mechanism for particular selectivity is also essential. Several protocols have been applied for engineering Cu-surface to tune the binding energies of the intermediates.[139-141] The introduction of the surface defects and atomic vacancies influences the electronic structure by adjusting the surrounding atoms, reducing energy barriers of intermediate reactions steps.[142] Similarly, the insertion of non-metal elements (S, P, N, or Se) into Cu structure can tune the electronic structure, surface defects, atomic vacancy, and modified local density of states. For example, the copper sulfide (CuS) structure presents stable defects and controlled surface vacancies such as point defects and strain. The introduction of the S atom into the Cu structure provides large modification in the local electron density of surface states which affects the CO binding.[143] In another example of the modified Cu_2S core with tuned Cu surface vacancies, the theoretical computation indicated that the presence of S atoms in Cu catalyst leads to a noticeable difference in the ratio of ethanol to ethylene for the CO_2 conversion to the C_2 pathway.[144] Besides, the multi-carbon products proceed through the dimerization or protonation of adsorbed CO intermediates. To this extent, the reduction of CO to ethanol presents a similar pathway to ethylene but involves three proton-electron coupled. At this point, $*C_2H_3O$ intermediate can protonate to ethanol or be left unprotonated to ethylene when the adsorbed oxygen atom is intact.[139] The thermodynamics of $*C_2H_3O$ intermediate can also be studied for ethylene to ethanol production. For the DFT study, the model system of pristine Cu slab and Cu slab with an atomic vacancy can be used for the reaction mechanism for the CO_2RR (**Figure 8a**).[144] In addition to $*C_2H_3O$ intermediate, the modified surface of the Cu core-shell and surface vacancies also

influence the reaction steps to form ethylene and ethanol. Thus, the theoretical findings can be translated to experimental results by forming surface defects and surface vacancies in the core-shell of sulfide-copper catalyst by using solvothermal synthesis. The controlled Cu surface vacancies (V-Cu_2S) for the CO_2RR yielded metallic Cu with enriched vacancies (**Figure 8b**), and the S and Cu are distributed evenly on the NP as depicted by EDS mapping (**Figure 8c-d**). The active catalyst was fabricated by electrochemical reduction of V-Cu_2S NPs, which helps remove the extra S on the surface to form Cu_2S-Cu-V. The core of Cu_2S consists of atomic vacancies. In these NPs, the Cu enriched the structure with low signals of S during CO_2RR (**Figure 8e-h**). Moreover, the S distribution was confirmed by EDS line scan, which exhibits S on the core of NPs as found in the picture of Cu_2S-Cu. Besides, the hollow structured CuS phase is also active for the CO_2RR to CO product at lower onset potential (~200 mV) with FE of 32.7%. The hollow cubic structure consisted of large exposed active sites and surface defects in favor of high catalytic activity.[145]

For other promising Cu-based catalysts with the elements insertion, copper nitride (Cu_3N) can also be applied as Cu^+ to promote CO_2RR. It is suggested that Cu_3N can tune Cu's electronic structure and surface, which reduces the energy barrier corresponding to the CO dimerization. The metallic Cu on the surface of Cu-on-Cu_3N promotes the production of C_{2+} products. Controlled synthesis of Cu_3N is a challenging task, octadecaylamine (ODA) ligands can be used to support the capping of Cu_3N. Besides, ligand exchange is another facile way to produce Cu on Cu_3N through oxidation of CuO-on-Cu_3N and then reduction to form Cu-on-Cu_3N crystals (**Figure 8i**).[121] Furthermore, the inner support of Cu_3N tuned the electronic structure of the Cu surface, which promoted the dimerization of the CO during CO_2RR. Additionally, the Cu_3N support suppressed the reduction of Cu^+ to obtain higher selectivity of C_{2+} products compared to Cu-on-

Cu_2O and pristine Cu. As a result, the C_{2+} products of C_2H_4, C_2H_5OH, and C_3H_7OH were found on Cu-on-Cu_3N at -0.95 V with FE of 39 ± 2%, 19 ± 1%, and 6 ± 1%, respectively, as presented in **Table 1**.

Moreover, modifying the Cu(111) surface by insertion of B is another thermodynamically favorable means for enhancing the formation of C_2 products during CO_2RR.[146] The CuB presents dendritic morphology with a 30-40 nm porous nanostructure. Inductive coupled plasma-optical emission spectroscopy (ICP-OES) quantity indicated that B/Cu atomic ratio was 2.7% to 5.7% with a measured depth of 7.5 nm. A large boron concentration was found within 2.5 nm depth of Cu catalysts. Furthermore, Bader charge analysis verified the electronic properties of boron-doped copper, which is a suitable material model for theoretical studies for electrical properties. The insertion of B into the surface of Cu slab exhibits the overlapping of binding states between Cu 2p and Cu 3d for CO adsorption on the surface of Cu compared to the original Cu surface. The d-band center of the neighboring Cu atom shifts away from the Fermi level than the pure Cu surface. The electron transfers from Cu to boron, resulting in oxidation of the Cu surface and geometric surface changes. In the boron-doped Cu (CuB) structure, both $Cu^{\delta+}$ and Cu^0 species existed. The presence of B dopant suppresses the C_1 reaction, enhances the C_2 product of C_2H_4 and C_2H_5OH under ambient conditions, and improves C_{2+} products by reducing the reaction energy for the rate-limiting step of *CO + *CO to OCCO*. The C_2 products were found on the CuB surface from CO_2RR with precise electron localization, which could be connected to the surface oxidation of Cu. These results arose from the synthesized boron-doped Cu with cubic phase with dominant peaks of (111) (**Figure 8j**).[146] Consequently, CuB presented superior activity for C_{2+} products as well as high stability for 40 h.

Furthermore, the insertion of Se into the Cu structure tuned the surface properties beneficial for the production of C_{2+} products. For example, $Cu_{1.8}Se$ NWs can easily be fabricated through chemical oxidation and selenization of $Cu(OH)_2$ NWs. The $Cu_{1.8}Se$ NWs are rough and consist of plenty of NPs because of the deformation through stretching. The $Cu_{1.8}Se$ NWs contained the lattice fringes of 0.33 nm, corresponding to (111) plane (**Figure 8k-m**).[147,148] Furthermore, EDS analysis confirms the elemental distribution of Cu and Se on the surface of $Cu_{1.8}Se$ NWs. The Se in $Cu_{1.8}Se$ NWs facilitates the high selectivity of the C_2 product in CO_2RR. Mainly, C_2H_4 and EtOH were found with FE of 55% and 24% at a voltage of -1.1 V, respectively, and the reaction was stable for 25 h at a current density of -14.6 mA cm^{-2}.[147,148] Besides metal selenides, metal phosphides are also active for the CO_2RR activity. There is an example of phosphorus (P) atom insertion into Cu structure to form Cu_3P NPs with controlled stoichiometry. The TEM, HRTEM, and SAED presented Cu_3P NPs of 8.7 ± 1.6 nm with an interlayer spacing of 0.21 and 0.36 nm corresponding to (110) planes (**Figure 8n-p**).[149] The CO_2RR on the surface of Cu_3P promotes the production of formate with an FE of 8% at -0.30 V. The surface chemistry of the Cu_3P provides the opportunity for higher selectivity of CO_2RR.

3.5 Single Cu Site Dispersed in Carbon Substrate

Cu-based electrocatalysts can reduce CO_2 to multi-carbon species because of the optimal binding energies of CO on the surface of Cu, which promotes further reduction to form C-C coupling for desirable products. Despite that, they still suffer a high resistance for the activation of the C-C coupling step. It is worth noting that the activity of electrocatalysts is contributed by the surface-active sites rather than the inner atoms, thus atomically dispersed catalysts with increased accessible active sites in the surface layers have emerged as promising candidates for a variety of applications. With regards to the CO_2RR, the maximized exposure of the Cu element can be

obtained for higher activity and selectivity through anchoring the single Cu atom in nitrogen-doped carbon (Cu-N-C), which modulates the electronic spin and enhances surface utilization.[25,69,150,151] The presence of single Cu site into the nitrogen-doped carbon (Cu-SA/NPC) framework can be confirmed by HAADF-STEM.[152] The bright dots presented the atomic distribution of Cu on Cu-SA/NPC catalysts without any large atomic clusters or particles (**Figure 9a**). The STEM mapping confirmed the elemental dispersion of Cu, N, and C in Cu-SA/NPC (**Figure 9b-e**).[152] Furthermore, the Cu atomic dispersion was substantiated by X-ray absorption near-edge spectroscopy (XANES) and extended X-ray absorption fine structure (EXAFS). Mostly, the Cu atom was assigned to the nitrogen atom by Cu-N bond, which affects the catalytic activity. For various coordination of N species, theoretical models could be constructed. A single Cu atom was anchored into a graphitic structure with pyridinic-N (Cu-pyridinic-N_4) and pyrrolic-N_4 (Cu-pyrrolic-N_4) as shown in **Figure 9f**.[152] The calculated Gibbs free energy of the intermediate steps for the CO_2RR presented the lowest energy pathways for the production of CH_3COCH_3 on the surface of Cu-pyridinic-N_4 and Cu-pyrrolic-N_4 at a particular potential of -0.36 V. Thus, it was observed that the change in energy of the overall process for the CO_2RR to CH_3COCH_3 was thermodynamically facile on the surface of Cu-SA/NPC catalysts, including the rate-limiting steps for the activation of CO_2 and *COOH (at 1.30 eV) for the CO_2RR. Furthermore, the lower value of ΔG (-1.06 eV) promotes the formation of *COOH on Cu-pyrrolic-N_4, which indicates that CO_2RR should be promoted by pyrrolic-N_4 on Cu-SA/NPC catalysts. Furthermore, the crucial step for the formation of C_2 product was based on two *CO for the C-C coupling with ΔG value of 1.67 eV and -1.23 eV on Cu-pyridinic-N_4 and Cu-pyrrolic-N_4, respectively, which evidence the quite facile route for C-C coupling through *CO on Cu-pyrrolic-N_4 sites.

In another example, Dilan *et al*. presented a Cu-N-C electrocatalyst with covalently integrated CuN_4 active sites into amorphous carbon structure for the CO_2RR to ethanol production.[153] In this study, CO was an authentic intermediate gas product, thus proving the catalyst's ability for electroreduction of CO to ethanol. The CuN_4 sites were also integrated into graphitic structure as revealed by EXAFS on copper-porphyrin (**Figure 9g**). Furthermore, bright dots dominated atomic dispersion into the carbon structure, representing the atomically dispersed nature of the Cu atoms (**Figure 9h**). In the same context, a single Cu atom was also dispersed in carbon nanofibers (CuSAs/CNFs) for the CO_2RR to methanol product, which provides maximum exposure of active sites.[154] Furthermore, a single atom of Cu dispersion was found in CuSAs/TCNFs under HAADF-STEM. The isolated Cu atoms were found on the nitrogen-doped carbon support well with Cu-N_4 moieties, agreeing well with XAFS results (**Figure 9i-l**).[154] This Cu-N_4 sites on the surface of CuSAs/TCNFs could convert the CO_2 to methanol with 44% FE and partial current density of -93 mA cm^{-2}. Moreover, the mechanistic involvement of the Cu-N_4 for the adsorption and reaction energies could be evaluated for the CO_2RR. The CO_2 conversion to *COOH is the rate-determining step on Cu-N_4 (1.17 eV) and pyridinic-N (1.62 eV). The C_1 products (*i.e.*, CH_3OH and CO) were observed in gaseous form, while no C_2 product was found, likely due to that an excess *CO intermediates blocked the C-C coupling. The CH_4 is also a potential C_1 product on the single Cu atomic site (**Figure 9m-p**).[154] However, the *COH intermediate would be further reduced to *CHOH with a particular energy barrier (~0.86 eV), instead of *C for the formation of CH_4 (**Figure 9q**).[154] In contrast, the intermediate reaction of *COH to C* presented a higher energy barrier (~1.88 eV) for the formation of CH_3OH, which is also higher than any steps in CH_3OH production. Therefore, the CuSAs/TCNFs promote the formation of CH_3OH as compared to CH_4

by facilitating the *CHOH formation. The synergistic effect of the holey carbon structure also contributed to the intermediate reaction step.[149]

3.6 Suboxide-Cu for the CO_2RR

The CO_2RR mechanism exhibits some unfavorable thermodynamics, making it necessary to identify the suitability and diversity of catalysts to produce hydrocarbons. For making catalysts, an atomistic understanding of adsorption and activation is included for the first step to initiate the reaction. Cu is a promising candidate for producing hydrocarbons, but Cu also needs high overpotential (>1 V) for the CO_2RR, unfavorable for fuel products. Although several works have been reported for the CO_2RR on the surface of Cu, considerable uncertainties remain to understand the role of Cu-surface to initiate the CO_2RR activity/selectivity. Also, a proton source is needed in the same reaction medium. Especially, water is the best solvent for the CO_2RR for sustainable solar-energy storage pathways. However, a comprehensive understanding of the absorption of CO_2RR and water molecules on the Cu surface is still needed. When the CO_2 adsorbs on the surface of Cu(111), the transient carbon-based species may start the reaction through chemisorption or physisorption of CO_2 on the surface, which was detailed discussed in the following subsection. To understand the reaction mechanism on the Cu-surface, electron-based spectroscopies can be studied to notify the adsorption process of CO_2, which are dependent on the particular temperature. For example, some electron spectroscopies were observed physisorption of CO_2 at 75 K, whereas chemisorption of CO_2 was done by partial negative induced charge through electronic capture ($CO_2^{\delta-}$). Liu *et al*. presented that the subsurface oxygen also plays a vital role for the production of C_{2+} by CO_2RR on the Cu-surface.[155] Theoretical studies have proved that canonical kinetics developed on subsurface oxygen during the CO_2RR could enhance the C-C coupling reaction. In contrast, the pure surface of Cu^0 leads to the fast HER reaction and suppresses the C_{2+} production.

The combined theoretical and time dependent-experimental contribution further determine the influence of subsurface oxygen for enhancing the C-C coupling on Cu catalysts. The rational development of Cu-surface under modified experimental conditions to secure subsurface oxygen is favorable for C_{2+} product formation under CO_2RR.

3.6.1 Chemisorbed CO_2 with H_2O on Cu(111)

When the CO_2 adsorb on the surface of Cu(111), only chemisorption occurs at room temperature. Similar *ex-situ* studies were done in ultrahigh vacuum (10-9 Torr) in low CO_2 flow at a particular temperature range (100 to 250 K), which did not evidence the CO_2-adsorption on the surface of Cu(100), Cu(110), and Cu(111). However, Nakamura *et al*. presented that CO_2 exposures of 65 to 650 Torr led to the build-up of atomically adsorbed oxygen at a rate which increased with temperature and decreased with reaction time at a temperature of 400 K to 600 K with an activation energy of 16 KJ mol^{-1}.[34] A similar phenomenon on clean Cu(111) under CO_2 flow of 740 Torr at a temperature of 475-550 K can also be studied. A lower CO_2 pressure of 0.05 Torr to 10 Torr showed CO_2 might dissociate on an oxidized-Cu surface.[156] Conclusively, CO_2 might dissociate quite easily on the peroxidic Cu surface, but no authentic evidence was found. CO_2-activation versus predicted chemisorbed CO_2 species was also presented on the stepped surface of Cu. However, *in-situ* characterization could not verify these species on the surface of Cu(111). These glitches and discrepancies present the importance of finding the initial species produced under the realistic gas pressures of CO_2 and H_2O.[34] Favaro *et al*. investigated the origin of CO_2 adsorption and presence of water on Cu(111) with suboxide surfaces ($Cu_{x=1.5,2.5}O$) separately *via in-situ* probing to predict the electronic and surface reaction using ambient-pressure X-ray photoelectron spectroscopy (APXPS) coupled soft X-rays (200-1,200 eV) at the solid/gas interface.[156] They discovered in particular that the existence of oxygenated species below the Cu surface and the

presence of water promote the adsorption/activation on the Cu surface. Additionally, water produces a tiny amount of suboxide to drive CO_2 adsorption through physisorption to chemisorption because water promotes the initiating of CO_2RR to formate products. The main exposed surface for Cu catalyst is Cu(111) orientation which was prepared from the polycrystalline sample by regular Ar sputtering and cycling followed by annealing under hydrogen flow at a temperature of 1100 K for one hour, which resulted in a distinct 1 × 1 surface as presented in low energy electron diffraction (LEED) analysis (**Figure 10a**).[156] The SEM images demonstrate the sputtering and annealing process, leading to the micro-level crystalline structure. APXPS characterized the sample without surface change through-beam diameter of ~0.8 mm. During *in-situ* APXPS testing at 298 K (**Figure 10b**),[156] initially, CO_2 pressure was 0.7 Torr on the particular metallic orientation of Cu(111) surface. For the second experiment, the surface was studied under 0.35 Torr, and CO_2 pressure was 0.7 Torr in the presence of H_2O. The APXPS measurement was carried out while dosing CO_2 on the metallic and suboxide surface of the Cu catalyst, where CO_2 and H_2O were joined without any contamination. The reactants (CO_2, H_2O, and O_2) were observed by quadrupole mass spectrometer (QMS), and no CO was present. Besides, the presence of subsurface oxygen corresponds to particular interaction within the gaseous phase. On the other hand, the existence of the C 1s spectral counterpart of formate and C-O(H) (**Figure 10c**) allowed us to build up a consistent O 1s fitting (**Figure 10d**). The gaseous water was aided by the formation of suboxide and converted to CO_2 adsorption from physisorbed to chemisorbed species to reduce CO_2 to the product of formate.

3.6.2 Physisorbed CO_2 with O on Cu-surface

The surface structure can be predicted for quarter monolayer equivalents of CO_2 on oxygen-free Cu(111) to understand the physisorption phenomenon (**Figure 10e-k**).[156] The molecular

physisorption of CO_2 presented C-O with a bond length of 1.164 Å compared to gaseous phase bond length of 1.163 Å. Additionally, O-C-O was at an angle of 179 with a balanced distance of 3.11 Å from carbon atom to CO_2 on the surface of Cu. In experimental studies, the observed shift in O 1s presented tiny surface or subsurface adsorbed (referred to as O_{ads} and O_{sub}) new Cu(111). In comparison, an experimental change in binding energies of adsorption oxygen (δO_{ads}) and subsurface adsorbed O (δO_{sub}) is −0.4 eV and −1.6 eV, respectively. Conclusively, the Cu catalysts produced surface oxides to improve the activity for the CO_2RR as compared to the metallic surface. Both experimental and theoretical findings verified that the outer layer of the Cu metallic needs to be exposed because CO_2 chemisorption activates the surface for the CO_2RR to formate (**Figure 10f**). However, the subsurface oxide was found to promote the water chemisorption on the Cu^+ center to promote the formate to formic acid under similar conditions. The oxidic subsurface plays a particular role in activating CO_2 and rationalizes a unique electrocatalyst for the CO_2RR.

3.7 Stability Issues with Cu-catalysts

It is understood that Cu is the only element that is electrochemically active for the CO_2RR to high-value multicarbon products. In the last two decades, great efforts have been devoted to the understanding of surface effects on catalytic performance for the CO_2RR, however, the insufficient stability of Cu-based catalysts for long-term operation is still a seious concern. For example, non-Cu catalysts exhibited stability up to 150 hours but most of the Cu-catalysts presented stability of a few minutes. It is crucial to know about the exact reasons behind the degradation mechanism but few reports have delivered that electrolyte impurities, poisoning of Cu-electrode, and blocking species reduced the FE of hydrocarbons after 10-30 min of CO_2RR. The surface deactivation could be due to heavy metal contamination, small contents of organic species, and reaction intermediates. For instance, a common example of the electrolyte for the CO_2RR is 0.1 M $KHCO_3$ consisting of

heavy metals like Fe, Zn, and Pb (0.02-0.05 ppm), which could deactivate the Cu surface.[157] Besides, the uncontrolled shape of the Cu-NPs lost their well-defined facets, reduced size under CO_2RR, and minimized the C-C coupling mechanism for C_{2+} products,[158] because the corners and edges presented a greater reaction tendency than on the flat surface. For the tiny clusters (2-4 nm), previous work manifested that the detachment from Cu-surface and their fragmentation,[114] coalescence, aggregation,[159] dissolution,[160] and Ostwald ripening is also the reason for degradation of activity for the CO_2RR (**Figure 11**).[82] It is very important to make stable Cu-catalysts with promising selectivity and activity to bring closer to commercial applications. To address these issues, the direct reconstruction or surface engineering Cu-catalysts through carbon coating could prevent the NPs agglomeration during CO_2RR.[57,161] Also, controlled morphology can be synthesized by using particular ligands (*e.g.*, thiols, triocytlphosphine oxide, strongly bonded carbenes, or amines) to regulate and optimize size and shapes.[162-164] However, there is still a need for more depth studies for engineering Cu-surface to reach out to the current demands and requirements of commercial applications.

4. TECHNO-ECONOMIC ANALYSIS FOR THE CO_2RR

The CO_2RR has drawn great attention in academic research as well as in industrial areas.[165] Experimentally, CO_2 is a primary source for the CO_2RR, and its purity has quite important for successful transformation to hydrocarbons. Logically, direct use of CO_2 industrial waste could not be applicable for a complicated CO_2RR to hydrocarbons because several additional impurities would stop the surface reactions and influence the practical applications. Therefore, CO_2 from industrial waste should be purified through efficient CO_2-separation materials or membranes and then be utilized as the reactants.[166,167] On the other hand, the techno-economic analysis at a large scale to meet the industry level for the production of hydrocarbon through CO_2RR on Cu-catalyst

is still unclear because of its long-term instability issue, poor selectivity and adequate FE of hydrocarbons. The advancement in synthetic strategies for producing stable Cu-catalysts is still needed to improve the selectivity, activity and stability for particular C_1 and C_2 products. Here we just reviewed current scenario of CO_2 electrolyzer technology for the formation of CO_2 conversion products. The improvements in CO_2RR to ethylene evidenced the profitability by techno-economic analyses. It was predicted that ethylene can be produced by 1000$/tonne with electrical energy efficiencies of ~52% through CO_2 to CO proceeding with CO to ethylene.[168,169] Besides, the low-temperature electrolyzer can be utilized for the CO_2RR to formic acid. While production of formic acid and CO needs high C-intensities with optimistic values of 137 g_{CO2}/kWh and 346 g_{CO2}/kWh, respectively.

Furthermore, the recycling pathway of CO_2 is electrolyzer consisting of CO_2RR and oxygen evolution reaction (OER), which are generally accepted as good sources for renewable energy. As a presumption, in the inexpensive electrolyzers as renewable energy resources, higher recycling rates for electrolytes and fixed operating parameters for CO_2RR-OER products have a positive economic impact compared to the commercial prices.[170] Each parameter for electrolyzer impacts the economics such as designs, gas diffusion layers (GDL), nafion cost, gaskets, bipolar graphite plates and membranes. It was assumed that 60% reduction in current market prices could scale up recyclability of CO_2. However, there is a need to adjust prices which have been reported in last few years. Schmidt *et al*. presented that engineered plant cost allows the adjustment of price from point to time.[170] The potential techno-economic values for low-temperature electrolyzers have been studied and concluded that father developments are still needed to make these technologies functional and beneficial for society. The advancement in external factors such as lower electricity,

CO_2 costs, internal factors of lower operating voltage, and higher current densities could improve the economical values for the CO_2RR to hydrocarbons.

5. CHALLENGES AND FUTURE PERSPECTIVES

In this review, we have summarized the strategies of surface engineering of Cu-catalysts and their effects on selectivity for the CO_2RR. The selectivity of Cu-surface for particular hydrocarbon products could be controlled by the tuned crystal structure, facet, composition (*e.g.*, Cu-alloy), and morphology. The individual surface presents different reaction tracks for the CO_2RR to hydrocarbons. Generally, common intermediates steps include *CO dimerization, C-C and C_1-C_2 coupling for the formation of C_2 and C_3 products, respectively. Although excellent work has been done on surface engineering Cu-based electrocatalysts over the past few decades, there is still a huge gap to bring these catalysts to the industry for carbon neutralization. The main challenge concerns the vast understanding and phenomenon behind catalysts for the selectivity of hydrocarbons. Surface engineering of Cu-catalysts by particular structure design, facet and shape for the CO_2RR is essential for higher selectivity for hydrocarbon products. The Cu-surface tuning with the coupling of secondary metal plays a role in reducing the energy barrier to enhance its activity and improve the interactions among intermediates such as *COOH, *CO, *CHO, *etc*. We recapitulated a few Cu-based bimetallic catalysts, which affect the H and O affinities, thus affecting the selectivity. This chemical composition among alloys enhances selectivity because of the correspondence linkage of binding energies of intermediates. Besides these general trends, more possible designs and surface tuning can be done for future Cu-catalysts to improve their electronic characteristics. Moreover, we have generalized the role of surface engineering of Cu for the CO_2RR to hydrocarbons and how to tune surface affects the activity and selectivity. Apart from

that, we also summarized how CO_2 exhibits both physisorption and chemisorption during the CO_2RR process.

The current literature survey found that an ideal catalyst for the CO_2RR should present the highest activity with the long period stability and selectivity of enormous FE for the particular required products. We suggest some key points to engineering the Cu-surface for the CO_2RR electrocatalyst to find a perfect motivation. (i) Effectively tuning Cu-surface with various approaches could enhance the active sites and improve the catalytic activity for the CO_2RR, for example, tuned Cu-structure (with particular phases) could provide targeted surface for specific selectivity of products, and ordered or disordered structure could improve surface area and accessible active sites for improved catalytic activity. (ii) Particular shape of Cu-surface streamlines various selectivity of products. Edges of the Cu-surface also affect the product selectivity because different shapes (such as cubic, dodecahedrons, and octahedrons) present different surface energy. Mostly, the cubic surface gives higher FE for ethylene products. (iii) Modified Cu-surface by the insertion of non-metal elements improves the electronic properties, promoting the surface energy for catalytic reactions. Non-metal element doped-Cu (*i.e.*, Cu_3N, CuB or CuS) was found to be highly active for the CO_2RR because of the tuned electronic behavior of Cu. Moreover, surface oxidation of Cu catalysts also promotes a higher FE for C_{2+} products. Additionally, there is a crucial need to locate the active sites for reaction intermediates and the coupling of C-C on the electrode/electrolyte interface. Therefore, operando techniques are needed for this deep understanding, such as XAS, XPS, FTIR, EC-STM, *etc*.

Although, several studies have been done on Cu-based electrocatalysts for the CO_2RR to hydrocarbon products, there are still many unresolved factors and challenges. For example, instability is a significant issue with Cu-electrocatalysts for the CO_2RR. The observed reasons

behind the instability are fragmentation, reshaping of NPs, agglomeration, detachment from the surface, and Ostwald ripening, which reduces the mass transport of protons and the reaction kinetics. Besides, the understanding of the origin of product selectivity on Cu-surface is still challenging. To this end, despite that, the ever-increasing research efforts in surface engineering of Cu-catalysts will continue to overcome the challenges mentioned above. Surface engineering Cu catalyst will also be helpful to achieve the targets for commercial applications of CO_2RR processes.

ACKNOWLEDGMENTS

The authors acknowledge the financial support from the National Science Foundation (CBET-1804326) and the University at Buffalo, the State University of New York.

AUTHOR CONTRIBUTIONS

G.W. and R.Z. conceptualized the review. H.T. investigated the literature and wrote the manuscript. G.W. and X.Y. revised the manuscript. All authors read, revised, and approved the submission of the final manuscript.

DECLARATION OF INTERESTS

The authors declare no competing interests.

REFERENCES

1. Schreier, M., Héroguel, F., Steier, L., Ahmad, S., Luterbacher, J.S., Mayer, M.T., Luo, J., and Grätzel, M. (2017). Solar conversion of CO_2 to CO using Earth-abundant electrocatalysts prepared by atomic layer modification of CuO. Nature Energy *2*, 17087.
2. Qiu, T., Gao, S., Liang, Z., Wang, D.-G., Tabassum, H., Zhong, R., and Zou, R. (2021). Pristine hollow metal-organic frameworks: design, synthesis and application. Angewandte Chemie International Edition *202012699*.
3. Tabassum, H., Guo, W., Meng, W., Mahmood, A., Zhao, R., Wang, Q., and Zou, R. (2017). Metal–Organic Frameworks Derived Cobalt Phosphide Architecture Encapsulated into B/N Co-Doped Graphene Nanotubes for All pH Value Electrochemical Hydrogen Evolution. Advanced Energy Materials *7*, 1601671.
4. Li, Y., Wang, H., Priest, C., Li, S., Xu, P., and Wu, G. (2021). Advanced Electrocatalysis for Energy and Environmental Sustainability via Water and Nitrogen Reactions. Advanced Materials *33*, 2000381.
5. Li, J., and Kornienko, N. (2021). Electrocatalytic carbon dioxide reduction in acid. Chem Catalysis *2*, 29-38.
6. Lin, S., Diercks, C.S., Zhang, Y.-B., Kornienko, N., Nichols, E.M., Zhao, Y., Paris, A.R., Kim, D., Yang, P., Yaghi, O.M., and Chang, C.J. (2015). Covalent organic frameworks comprising cobalt porphyrins for catalytic CO_2 reduction in water. Science *349*, 1208.
7. Tabassum, H., Mahmood, A., Zhu, B., Liang, Z., Zhong, R., Guo, S., and Zou, R. (2019). Recent advances in confining metal-based nanoparticles into carbon nanotubes for electrochemical energy conversion and storage devices. Energy & Environmental Science *12*, 2924-2956.

8. Kim, M.J., Cruz, M.A., Yang, F., and Wiley, B.J. (2019). Accelerating electrochemistry with metal nanowires. Current Opinion in Electrochemistry *16*, 19-27.

9. Tabassum, H., Zou, R., Mahmood, A., Liang, Z., Wang, Q., Zhang, H., Gao, S., Qu, C., Guo, W., and Guo, S. (2018). A Universal Strategy for Hollow Metal Oxide Nanoparticles Encapsulated into B/N Co-Doped Graphitic Nanotubes as High-Performance Lithium-Ion Battery Anodes. Advanced Materials *30*, 1705441.

10. Mahmood, A., Ali, Z., Tabassum, H., Akram, A., Aftab, W., Ali, R., Khan, M.W., Loomba, S., Alluqmani, A., Adil Riaz, M., et al. (2020). Carbon Fibers Embedded With Iron Selenide (Fe_3Se_4) as Anode for High-Performance Sodium and Potassium Ion Batteries. Frontiers in Chemistry *8*.

11. Tabassum, H., Qu, C., Cai, K., Aftab, W., Liang, Z., Qiu, T., Mahmood, A., Meng, W., and Zou, R. (2018). Large-scale fabrication of BCN nanotube architecture entangled on a three-dimensional carbon skeleton for energy storage. Journal of Materials Chemistry A *6*, 21225-21230.

12. Tabassum, H., Zou, R., Mahmood, A., Liang, Z., and Guo, S. (2016). A catalyst-free synthesis of B, N co-doped graphene nanostructures with tunable dimensions as highly efficient metal free dual electrocatalysts. Journal of Materials Chemistry A *4*, 16469-16475.

13. Tabassum, H., Zhi, C., Wu, Y., Zhong, R., Hussain, T., Qiu, T., Tang, Y., Liang, Z., Guo, W., and Zou, R. (2021). Rationalized atomic/clusters dispersion of Fe/Se/Al on interconnected N-doped carbon nanofibers for fast sodiation. Chemical Engineering Journal *411*, 128420.

14. Zhang, X., Deng, J., Pupucevski, M., Impeng, S., Yang, B., Chen, G., Kuboon, S., Zhong, Q., Faungnawakij, K., Zheng, L., et al. (2021). High-Performance Binary Mo–Ni Catalysts for Efficient Carbon Removal during Carbon Dioxide Reforming of Methane. ACS Catalysis *11*, 12087-12095.

15. Majeed, A., Hou, P.-X., Zhang, F., Tabassum, H., Li, X., Li, G.-X., Liu, C., and Cheng, H.-M. (2019). A Freestanding Single-Wall Carbon Nanotube Film Decorated with N-Doped Carbon-Encapsulated Ni Nanoparticles as a Bifunctional Electrocatalyst for Overall Water Splitting. Advanced Science *6*, 1802177.

16. Schouten, K.J.P., Qin, Z., Pérez Gallent, E., and Koper, M.T.M. (2012). Two Pathways for the Formation of Ethylene in CO Reduction on Single-Crystal Copper Electrodes. Journal of the American Chemical Society *134*, 9864-9867.

17. Xie, H., Wan, Y., Wang, X., Liang, J., Lu, G., Wang, T., Chai, G., Adli, N.M., Priest, C., Huang, Y., et al. (2021). Boosting Pd-catalysis for electrochemical CO_2 reduction to CO on Bi-Pd single atom alloy nanodendrites. Applied Catalysis B: Environmental *289*, 119783.

18. Zhang, Y., Wang, X., Zheng, S., Yang, B., Li, Z., Lu, J., Zhang, Q., Adli, N.M., Lei, L., Wu, G., and Hou, Y. (2021). Hierarchical Cross-Linked Carbon Aerogels with Transition Metal-Nitrogen Sites for Highly Efficient Industrial-Level CO_2 Electroreduction. Advanced Functional Materials *31*, 2104377.

19. Pan, F., Zhang, H., Liu, K., Cullen, D., More, K., Wang, M., Feng, Z., Wang, G., Wu, G., and Li, Y. (2018). Unveiling Active Sites of CO_2 Reduction on Nitrogen-Coordinated and Atomically Dispersed Iron and Cobalt Catalysts. ACS Catalysis *8*, 3116-3122.

20. Shi, Q., Hwang, S., Yang, H., Ismail, F., Su, D., Higgins, D., and Wu, G. (2020). Supported and coordinated single metal site electrocatalysts. Materials Today *37*, 93-111.

21. He, Y., Shi, Q., Shan, W., Li, X., Kropf, A.J., Wegener, E.C., Wright, J., Karakalos, S., Su, D., Cullen, D.A., et al. (2021). Dynamically Unveiling Metal-Nitrogen Coordination during Thermal Activation to Design High-Efficient Atomically Dispersed CoN_4 Active Sites. Angew Chem Int Ed Engl *60*, 9516-9526.

22. Yang, X., Wang, M., Zachman, M.J., Zhou, H., He, Y., Liu, S., Zang, H.-Y., Feng, Z., and Wu, G. (2021). Binary Atomically Dispersed Metal-Site Catalysts with Core−Shell Nanostructures for O_2 and CO_2 Reduction Reactions. Small Science *1*, 2100046.

23. Shi, Q., He, Y., Bai, X., Wang, M., Cullen, D.A., Lucero, M., Zhao, X., More, K.L., Zhou, H., Feng, Z., et al. (2020). Methanol tolerance of atomically dispersed single metal site catalysts: mechanistic understanding and high-performance direct methanol fuel cells. Energy & Environmental Science *13*, 3544-3555.

24. Kuhl, K.P., Cave, E.R., Abram, D.N., and Jaramillo, T.F. (2012). New insights into the electrochemical reduction of carbon dioxide on metallic copper surfaces. Energy & Environmental Science *5*, 7050-7059.

25. Chen, Z., Liao, X., Sun, C., Zhao, K., Ye, D., Li, J., Wu, G., Fang, J., Zhao, H., and Zhang, J. (2021). Enhanced performance of atomically dispersed dual-site Fe-Mn electrocatalysts through cascade reaction mechanism. Applied Catalysis B: Environmental *288*.

26. Lee, S.H., Lin, J.C., Farmand, M., Landers, A.T., Feaster, J.T., Avilés Acosta, J.E., Beeman, J.W., Ye, Y., Yano, J., Mehta, A., et al. (2021). Oxidation State and Surface Reconstruction of Cu under CO_2 Reduction Conditions from In Situ X-ray Characterization. Journal of the American Chemical Society *143*, 588-592.

27. Lee, S.Y., Jung, H., Kim, N.-K., Oh, H.-S., Min, B.K., and Hwang, Y.J. (2018). Mixed Copper States in Anodized Cu Electrocatalyst for Stable and Selective Ethylene Production from CO_2 Reduction. Journal of the American Chemical Society *140*, 8681-8689.

28. Li, X., He, Y., Cheng, S., Li, B., Zeng, Y., Xie, Z., Meng, Q., Ma, L., Kisslinger, K., Tong, X., et al. (2021). Atomic Structure Evolution of Pt-Co Binary Catalysts: Single Metal Sites versus Intermetallic Nanocrystals. Adv Mater *33*, e2106371.

29. Kim, Y.-G., Baricuatro, J.H., Javier, A., Gregoire, J.M., and Soriaga, M.P. (2014). The evolution of the polycrystalline copper surface, first to Cu (111) and then to Cu (100), at a fixed CO_2RR potential: A study by operando EC-STM. Langmuir *30*, 15053-15056.

30. Zhang, J., Yang, H., Gao, J., Xi, S., Cai, W., Zhang, J., Cui, P., and Liu, B. (2020). Design of hierarchical, three-dimensional free-standing single-atom electrode for H_2O_2 production in acidic media. Carbon Energy *2*, 276-282.

31. Zhao, Y., Chang, X., Malkani, A.S., Yang, X., Thompson, L., Jiao, F., and Xu, B. (2020). Speciation of Cu Surfaces During the Electrochemical CO Reduction Reaction. Journal of the American Chemical Society *142*, 9735-9743.

32. Nitopi, S., Bertheussen, E., Scott, S.B., Liu, X., Engstfeld, A.K., Horch, S., Seger, B., Stephens, I.E.L., Chan, K., Hahn, C., et al. (2019). Progress and Perspectives of Electrochemical CO_2 Reduction on Copper in Aqueous Electrolyte. Chemical Reviews *119*, 7610-7672.

33. Hori, Y., Kikuchi, K., Murata, A., and Suzuki, S. (1986). Production Of Methane And Ethylene In Electrochemical Reduction Of Carbon Dioxide At Copper Electrode In Aqueous Hydrogencarbonate Solution. Chemistry Letters *15*, 897-898.

34. Nakamura, J., Rodriguez, J.A., and Campbell, C.T. (1989). Does CO_2dissociatively adsorb on Cu surfaces? Journal of Physics: Condensed Matter *1*, 149-160.

35. Zhang, W., Jin, Z., and Chen, Z. (2022). Rational-Designed Principles for Electrochemical and Photoelectrochemical Upgrading of CO_2 to Value-Added Chemicals. Advanced Science, 2105204.

36. Fang, H.-X., Guo, H., Niu, C.-G., Liang, C., Huang, D.-W., Tang, N., Liu, H.-Y., Yang, Y.-Y., and Li, L. (2020). Hollow tubular graphitic carbon nitride catalyst with adjustable nitrogen vacancy: Enhanced optical absorption and carrier separation for improving photocatalytic activity. Chemical Engineering Journal *402*, 126185.

37. Arán-Ais, R.M., Gao, D., and Roldan Cuenya, B. (2018). Structure- and Electrolyte-Sensitivity in CO_2 Electroreduction. Accounts of Chemical Research *51*, 2906-2917.

38. Vasileff, A., Xu, C., Jiao, Y., Zheng, Y., and Qiao, S.-Z. (2018). Surface and Interface Engineering in Copper-Based Bimetallic Materials for Selective CO_2 Electroreduction. Chem *4*, 1809-1831.

39. Hori, Y., Takahashi, R., Yoshinami, Y., and Murata, A. (1997). Electrochemical Reduction of CO at a Copper Electrode. The Journal of Physical Chemistry B *101*, 7075-7081.

40. Hori, Y., Takahashi, I., Koga, O., and Hoshi, N. (2002). Selective Formation of C_2 Compounds from Electrochemical Reduction of CO_2 at a Series of Copper Single Crystal Electrodes. The Journal of Physical Chemistry B *106*, 15-17.

41. Zhang, Z., Bian, L., Tian, H., Liu, Y., Bando, Y., Yamauchi, Y., and Wang, Z.-L. (2022). Tailoring the Surface and Interface Structures of Copper-Based Catalysts for Electrochemical Reduction of CO_2 to Ethylene and Ethanol. Small, 2107450.

42. Wen, C.F., Zhou, M., Liu, P.F., Liu, Y., Wu, X., Mao, F., Dai, S., Xu, B., Wang, X.L., Jiang, Z., et al. (2022). Highly Ethylene-Selective Electrocatalytic CO_2 Reduction Enabled by Isolated Cu−S Motifs in Metal–Organic Framework Based Precatalysts. Angewandte Chemie International Edition *61*, 202111700.

43. Woldu, A.R., Huang, Z., Zhao, P., Hu, L., and Astruc, D. (2022). Electrochemical CO_2 reduction (CO_2RR) to multi-carbon products over copper-based catalysts. Coordination Chemistry Reviews *454*, 214340.

44. Rossi, K., and Buonsanti, R. (2022). Shaping Copper Nanocatalysts to Steer Selectivity in the Electrochemical CO_2 Reduction Reaction. Accounts of Chemical Research, doi.org/10.1021/acs.accounts.1021c00673.

45. Ummireddi, A.K., Sharma, S.K., and Pala, R.G.S. (2022). Ammonium ionic liquid cation promotes electrochemical CO_2 reduction to ethylene over formate while inhibiting the hydrogen evolution on a copper electrode. Catalysis Science & Technology *12*, 519-529.

46. Hung, S.-F., Wu, F.-Y., Lu, Y.-H., Lee, T.-J., Tsai, H.-J., Chen, P.-H., Lin, Z.-Y., Chen, G.-L., Huang, W.-Y., and Zeng, W.-J. (2022). Operando X-ray Absorption Spectroscopic Studies of Carbon Dioxide Reduction Reaction in a Modified Flow Cell. Catalysis Science & Technology.

47. Yan, X., Chen, C., Wu, Y., Chen, Y., Zhang, J., Feng, R., Zhang, J., and Han, B. (2022). Boosting CO_2 electroreduction to C_{2+} products on fluorine-doped copper. Green Chemistry.

48. Lawrence, M.J., Celorrio, V., Sargeant, E., Huang, H., Rodríguez-López, J., Zhu, Y., Gu, M., Russell, A.E., and Rodriguez, P. (2022). Insight into the Activity and Selectivity of Nanostructured Copper Titanates during Electrochemical Conversion of CO_2 at Neutral pH

via In Situ X-ray Absorption Spectroscopy. ACS Applied Materials & Interfaces *14*, 2742-2753.

49. Choi, W., Park, S., Jung, W., Won, D.H., Na, J., and Hwang, Y.J. (2022). Origin of Hydrogen Incorporated into Ethylene during Electrochemical CO_2 Reduction in Membrane Electrode Assembly. ACS Energy Letters, 939-945.

50. Daems, N., Choukroun, D., Merino, P., Rettenmaier, C., Pacquets, L., Bergmann, A., Santoro, G., Vázquez, L., Martínez, L., Roldan Cuenya, B., et al. (2022). Steering Hydrocarbon Selectivity in CO_2 Electroreduction over Soft-Landed CuOx Nanoparticle-Functionalized Gas Diffusion Electrodes. ACS Applied Materials & Interfaces *14*, 2691-2702.

51. Liang, J., Ma, F., Hwang, S., Wang, X., Sokolowski, J., Li, Q., Wu, G., and Su, D. (2019). Atomic Arrangement Engineering of Metallic Nanocrystals for Energy-Conversion Electrocatalysis. Joule *3*, 956-991.

52. Altaf, N., Liang, S., Huang, L., and Wang, Q. (2020). Electro-derived Cu-Cu_2O nanocluster from LDH for stable and selective C_2 hydrocarbons production from CO_2 electrochemical reduction. Journal of Energy Chemistry *48*, 169-180.

53. Zhao, X., Yang, X., Wang, M., Hwang, S., Karakalos, S., Chen, M., Qiao, Z., Wang, L., Liu, B., Ma, Q., et al. (2020). Single-Iron Site Catalysts with Self-Assembled Dual-size Architecture and Hierarchical Porosity for Proton-Exchange Membrane Fuel Cells. Applied Catalysis B: Environmental *279*, 119400.

54. Garza, A.J., Bell, A.T., and Head-Gordon, M. (2018). Mechanism of CO_2 Reduction at Copper Surfaces: Pathways to C_2 Products. ACS Catalysis *8*, 1490-1499.

55. Fan, Q., Zhang, M., Jia, M., Liu, S., Qiu, J., and Sun, Z. (2018). Electrochemical CO_2 reduction to C_{2+} species: Heterogeneous electrocatalysts, reaction pathways, and optimization strategies. Materials Today Energy *10*, 280-301.

56. Li, J., Zhang, H., Samarakoon, W., Shan, W., Cullen, D.A., Karakalos, S., Chen, M., Gu, D., More, K.L., Wang, G., et al. (2019). Thermally Driven Structure and Performance Evolution of Atomically Dispersed FeN_4 Sites for Oxygen Reduction. Angewandte Chemie International Edition *58*, 18971-18980.

57. Gao, D., Arán-Ais, R.M., Jeon, H.S., and Roldan Cuenya, B. (2019). Rational catalyst and electrolyte design for CO_2 electroreduction towards multicarbon products. Nature Catalysis *2*, 198-210.

58. Zheng, Y., Vasileff, A., Zhou, X., Jiao, Y., Jaroniec, M., and Qiao, S.-Z. (2019). Understanding the Roadmap for Electrochemical Reduction of CO_2 to Multi-Carbon Oxygenates and Hydrocarbons on Copper-Based Catalysts. Journal of the American Chemical Society *141*, 7646-7659.

59. Handoko, A.D., Chan, K.W., and Yeo, B.S. (2017). –CH3 Mediated Pathway for the Electroreduction of CO_2 to Ethane and Ethanol on Thick Oxide-Derived Copper Catalysts at Low Overpotentials. ACS Energy Letters *2*, 2103-2109.

60. Jouny, M., Luc, W., and Jiao, F. (2018). High-rate electroreduction of carbon monoxide to multi-carbon products. Nature Catalysis *1*, 748-755.

61. Calle-Vallejo, F., and Koper, M.T.M. (2013). Theoretical Considerations on the Electroreduction of CO to C_2 Species on Cu(100) Electrodes. Angewandte Chemie International Edition *52*, 7282-7285.

62. Pérez-Gallent, E., Figueiredo, M.C., Calle-Vallejo, F., and Koper, M.T.M. (2017). Spectroscopic Observation of a Hydrogenated CO Dimer Intermediate During CO Reduction on Cu(100) Electrodes. Angewandte Chemie International Edition *56*, 3621-3624.

63. Schouten, K.J.P., Kwon, Y., van der Ham, C.J.M., Qin, Z., and Koper, M.T.M. (2011). A new mechanism for the selectivity to C_1 and C_2 species in the electrochemical reduction of carbon dioxide on copper electrodes. Chemical Science *2*, 1902-1909.

64. Hanselman, S., Koper, M.T.M., and Calle-Vallejo, F. (2018). Computational Comparison of Late Transition Metal (100) Surfaces for the Electrocatalytic Reduction of CO to C_2 Species. ACS Energy Letters *3*, 1062-1067.

65. Clark, E.L., and Bell, A.T. (2018). Direct Observation of the Local Reaction Environment during the Electrochemical Reduction of CO_2. Journal of the American Chemical Society *140*, 7012-7020.

66. Zhuang, T.-T., Pang, Y., Liang, Z.-Q., Wang, Z., Li, Y., Tan, C.-S., Li, J., Dinh, C.T., De Luna, P., Hsieh, P.-L., et al. (2018). Copper nanocavities confine intermediates for efficient electrosynthesis of C_3 alcohol fuels from carbon monoxide. Nature Catalysis *1*, 946-951.

67. Kibria, M.G., Dinh, C.-T., Seifitokaldani, A., De Luna, P., Burdyny, T., Quintero-Bermudez, R., Ross, M.B., Bushuyev, O.S., García de Arquer, F.P., Yang, P., et al. (2018). A Surface Reconstruction Route to High Productivity and Selectivity in CO_2 Electroreduction toward C2+ Hydrocarbons. Advanced Materials *30*, 1804867.

68. Ratschmeier, B., Kemna, A., and Braunschweig, B. (2020). Role of H_2O for CO_2 Reduction Reactions at Platinum/Electrolyte Interfaces in Imidazolium Room-Temperature Ionic Liquids. ChemElectroChem *7*, 1765-1774.

69. Wang, Y., Zhu, Y., and Niu, C. (2020). Surface and length effects for aqueous electrochemical reduction of CO_2 as studied over copper nanowire arrays. Journal of Physics and Chemistry of Solids *144*, 109507.

70. Hu, Z., and Boyd, R.J. (2000). Structure sensitivity and cluster size convergence for formate adsorption on copper surfaces: A DFT cluster model study. The Journal of Chemical Physics *112*, 9562-9568.

71. Wen, G., Ren, B., Zheng, Y., Li, M., Silva, C., Song, S., Zhang, Z., Dou, H., Zhao, L., Luo, D., et al. (2022). Engineering Electrochemical Surface for Efficient Carbon Dioxide Upgrade. Advanced Energy Materials *12*, 2103289.

72. Xiang, K., Shen, F., Fu, Y., Wu, L., Wang, Z., Yi, H., Liu, X., Wang, P., Liu, M., Lin, Z., and Liu, H. (2022). Boosting CO_2 electroreduction towards C_{2+} products via CO* intermediate manipulation on copper-based catalysts. Environmental Science: Nano.

73. Tang, T., Wang, Z., and Guan, J. (2022). Optimizing the Electrocatalytic Selectivity of Carbon Dioxide Reduction Reaction by Regulating the Electronic Structure of Single-Atom M-N-C Materials. Advanced Functional Materials *n/a*, 2111504.

74. Zhang, W., Huang, C., Zhu, J., Zhou, Q., Yu, R., Wang, Y., An, P., Zhang, J., Qiu, M., Zhou, L., et al. (2022). Dynamic Restructuring of Coordinatively Unsaturated Copper Paddle Wheel Clusters to Boost Electrochemical CO_2 Reduction to Hydrocarbons**. Angewandte Chemie International Edition *61*, e202112116.

75. Li, Y., Cui, F., Ross, M.B., Kim, D., Sun, Y., and Yang, P. (2017). Structure-Sensitive CO_2 Electroreduction to Hydrocarbons on Ultrathin 5-fold Twinned Copper Nanowires. Nano Letters *17*, 1312-1317.

76. Zhang, W., Hu, Y., Ma, L., Zhu, G., Wang, Y., Xue, X., Chen, R., Yang, S., and Jin, Z. (2018). Progress and perspective of electrocatalytic CO_2 reduction for renewable carbonaceous fuels and chemicals. Advanced Science *5*, 1700275.

77. Wang, Z., Yang, G., Zhang, Z., Jin, M., and Yin, Y. (2016). Selectivity on Etching: Creation of High-Energy Facets on Copper Nanocrystals for CO_2 Electrochemical Reduction. ACS Nano *10*, 4559-4564.

78. Li, Q., Zhu, W., Fu, J., Zhang, H., Wu, G., and Sun, S. (2016). Controlled assembly of Cu nanoparticles on pyridinic-N rich graphene for electrochemical reduction of CO_2 to ethylene. Nano Energy *24*, 1-9.

79. Ding, T., Liu, X., Tao, Z., Liu, T., Chen, T., Zhang, W., Shen, X., Liu, D., Wang, S., Pang, B., et al. (2021). Atomically Precise Dinuclear Site Active toward Electrocatalytic CO_2 Reduction. J Am Chem Soc *143*, 11317-11324.

80. Hahn, C., Hatsukade, T., Kim, Y.-G., Vailionis, A., Baricuatro, J.H., Higgins, D.C., Nitopi, S.A., Soriaga, M.P., and Jaramillo, T.F. (2017). Engineering Cu surfaces for the electrocatalytic conversion of CO_2: Controlling selectivity toward oxygenates and hydrocarbons. Proceedings of the National Academy of Sciences, 201618935.

81. Raciti, D., Cao, L., Livi, K.J.T., Rottmann, P.F., Tang, X., Li, C., Hicks, Z., Bowen, K.H., Hemker, K.J., Mueller, T., and Wang, C. (2017). Low-Overpotential Electroreduction of Carbon Monoxide Using Copper Nanowires. ACS Catalysis *7*, 4467-4472.

82. Popović, S., Smiljanić, M., Jovanovič, P., Vavra, J., Buonsanti, R., and Hodnik, N. (2020). Stability and Degradation Mechanisms of Copper-Based Catalysts for Electrochemical CO_2 Reduction. Angewandte Chemie International Edition *59*, 14736-14746.

83. Xiao, H., Goddard, W.A., Cheng, T., and Liu, Y. (2017). Cu metal embedded in oxidized matrix catalyst to promote CO_2 activation and CO dimerization for electrochemical reduction of CO_2. Proceedings of the National Academy of Sciences *114*, 6685.

84. Chou, T.-C., Chang, C.-C., Yu, H.-L., Yu, W.-Y., Dong, C.-L., Velasco-Vélez, J.-J., Chuang, C.-H., Chen, L.-C., Lee, J.-F., Chen, J.-M., and Wu, H.-L. (2020). Controlling the Oxidation State of the Cu Electrode and Reaction Intermediates for Electrochemical CO_2 Reduction to Ethylene. Journal of the American Chemical Society *142*, 2857-2867.

85. Velasco-Vélez, J.-J., Jones, T., Gao, D., Carbonio, E., Arrigo, R., Hsu, C.-J., Huang, Y.-C., Dong, C.-L., Chen, J.-M., Lee, J.-F., et al. (2019). The Role of the Copper Oxidation State in the Electrocatalytic Reduction of CO_2 into Valuable Hydrocarbons. ACS Sustainable Chemistry & Engineering *7*, 1485-1492.

86. Lee, S.H., Sullivan, I., Larson, D.M., Liu, G., Toma, F.M., Xiang, C., and Drisdell, W.S. (2020). Correlating Oxidation State and Surface Area to Activity from Operando Studies of Copper CO Electroreduction Catalysts in a Gas-Fed Device. ACS Catalysis *10*, 8000-8011.

87. Kim, Y.-G., Baricuatro, J.H., and Soriaga, M.P. (2018). Surface Reconstruction of Polycrystalline Cu Electrodes in Aqueous $KHCO_3$ Electrolyte at Potentials in the Early Stages of CO_2 Reduction. Electrocatalysis *9*, 526-530.

88. Yano, J., and Yamasaki, S. (2008). Pulse-mode electrochemical reduction of carbon dioxide using copper and copper oxide electrodes for selective ethylene formation. Journal of Applied Electrochemistry *38*, 1721.

89. Huang, J., Mensi, M., Oveisi, E., Mantella, V., and Buonsanti, R. (2019). Structural Sensitivities in Bimetallic Catalysts for Electrochemical CO_2 Reduction Revealed by Ag–Cu Nanodimers. Journal of the American Chemical Society *141*, 2490-2499.

90. Arán-Ais, R.M., Scholten, F., Kunze, S., Rizo, R., and Roldan Cuenya, B. (2020). The role of in situ generated morphological motifs and Cu(i) species in C_{2+} product selectivity during CO_2 pulsed electroreduction. Nature Energy *5*, 317-325.

91. Mistry, H., Varela, A.S., Bonifacio, C.S., Zegkinoglou, I., Sinev, I., Choi, Y.-W., Kisslinger, K., Stach, E.A., Yang, J.C., Strasser, P., and Cuenya, B.R. (2016). Highly selective plasma-activated copper catalysts for carbon dioxide reduction to ethylene. Nature Communications *7*, 12123.

92. Zhang, J., Luo, W., and Züttel, A. (2019). Self-supported copper-based gas diffusion electrodes for CO_2 electrochemical reduction. Journal of Materials Chemistry A *7*, 26285-26292.

93. Sen, S., Liu, D., and Palmore, G.T.R. (2014). Electrochemical Reduction of CO_2 at Copper Nanofoams. ACS Catalysis *4*, 3091-3095.

94. Zarandi, R.F., Rezaei, B., Ghaziaskar, H.S., and Ensafi, A.A. (2019). Electrochemical reduction of CO_2 to ethanol using copper nanofoam electrode and 1-butyl-3-methyl-imidazolium bromide as the homogeneous co-catalyst. Journal of Environmental Chemical Engineering *7*, 103141.

95. Jiang, K., Huang, Y., Zeng, G., Toma, F.M., Goddard, W.A., and Bell, A.T. (2020). Effects of Surface Roughness on the Electrochemical Reduction of CO_2 over Cu. ACS Energy Letters *5*, 1206-1214.

96. Huang, Y., Chen, Y., Cheng, T., Wang, L.-W., and Goddard, W.A. (2018). Identification of the Selective Sites for Electrochemical Reduction of CO to C_{2+} Products on Copper Nanoparticles by Combining Reactive Force Fields, Density Functional Theory, and Machine Learning. ACS Energy Letters *3*, 2983-2988.

97. Gao, D., McCrum, I.T., Deo, S., Choi, Y.-W., Scholten, F., Wan, W., Chen, J.G., Janik, M.J., and Roldan Cuenya, B. (2018). Activity and Selectivity Control in CO_2 Electroreduction to Multicarbon Products over CuOx Catalysts via Electrolyte Design. ACS Catalysis *8*, 10012-10020.

98. Basiratnia, A., Rempel, J., Li, F., Pogodaev, A., Zienchuk, T.A., and Klinkova, A. (2019). Cu(ii)-nanoparticle-derived structures under CO_2 reduction conditions: a matter of shape. Physical Chemistry Chemical Physics *21*, 5894-5897.

99. Liu, D., Wang, B., Li, H., Huang, S., Liu, M., Wang, J., Wang, Q., Zhang, J., and Zhao, Y. (2019). Distinguished Zn,Co-N_x-C-S_y active sites confined in dentric carbon for highly efficient oxygen reduction reaction and flexible Zn-air Batteries. Nano Energy *58*, 277-283.

100. Lai, W., Ma, Z., Zhang, J., Yuan, Y., Qiao, Y., and Huang, H. (2022). Dynamic Evolution of Active Sites in Electrocatalytic CO_2 Reduction Reaction: Fundamental Understanding and Recent Progress. Advanced Functional Materials *n/a*, 2111193.

101. Banerjee, S., Gerke, C.S., and Thoi, V.S. (2022). Guiding CO2RR Selectivity by Compositional Tuning in the Electrochemical Double Layer. Accounts of Chemical Research *55*, 504-515.

102. Chang, Y.-B., Zhang, C., Lu, X.-L., Zhang, W., and Lu, T.-B. (2022). Graphdiyene enables ultrafine Cu nanoparticles to selectively reduce CO_2 to C_{2+} products. Nano Research *15*, 195-201.

103. Zhao, Z., Pang, L., Su, Y., Liu, T., Wang, G., Liu, C., Wang, J., and Peng, Z. (2022). Deciphering CO_2 Reduction Reaction Mechanism in Aprotic Li–CO_2 Batteries using In Situ Vibrational Spectroscopy Coupled with Theoretical Calculations. ACS Energy Letters *7*, 624-631.

104. Yu, S., Louisia, S., and Yang, P. (2022). The Interactive Dynamics of Nanocatalyst Structure and Microenvironment during Electrochemical CO_2 Conversion. JACS Au.

105. Li, H., Yue, X., Che, J., Xiao, Z., Yu, X., Sun, F., Xue, C., and Xiang, J. (2022). High Performance 3D Self-Supporting Cu−Bi Aerogels for Electrocatalytic Reduction of CO_2 to Formate. ChemSusChem *n/a*, e202200226.

106. Ooka, H., Figueiredo, M.C., and Koper, M.T.M. (2017). Competition between Hydrogen Evolution and Carbon Dioxide Reduction on Copper Electrodes in Mildly Acidic Media. Langmuir *33*, 9307-9313.

107. Sikdar, N., Junqueira, J.R.C., Öhl, D., Dieckhöfer, S., Quast, T., Braun, M., Aiyappa, H.B., Seisel, S., Andronescu, C., and Schuhmann, W. (2022). Redox Replacement of Silver on MOF-Derived Cu/C Nanoparticles on Gas Diffusion Electrodes for Electrocatalytic CO_2 Reduction. Chemistry – A European Journal *28*, e202104249.

108. Fu, W., Liu, Z., Wang, T., Liang, J., Duan, S., Xie, L., Han, J., and Li, Q. (2020). Promoting C_{2+} Production from Electrochemical CO_2 Reduction on Shape-Controlled Cuprous Oxide Nanocrystals with High-Index Facets. ACS Sustainable Chemistry & Engineering *8*, 15223-15229.

109. Takahashi, I., Koga, O., Hoshi, N., and Hori, Y. (2002). Electrochemical reduction of CO_2 at copper single crystal Cu(S)-[n(111)×(111)] and Cu(S)-[n(110)×(100)] electrodes. Journal of Electroanalytical Chemistry *533*, 135-143.

110. Li, C.W., Ciston, J., and Kanan, M.W. (2014). Electroreduction of carbon monoxide to liquid fuel on oxide-derived nanocrystalline copper. Nature *508*, 504-507.

111. He, X., He, R., Lan, Q., Duan, F., Xiao, J., Song, M., Zhang, M., Chen, Y., and Li, Y. (2016). A Facile Fabrication of Silver-Coated Copper Nanowires by Galvanic Replacement. Journal of Nanomaterials *2016*, 2127980.

112. Kwon, Y., Lum, Y., Clark, E.L., Ager, J.W., and Bell, A.T. (2016). CO_2 Electroreduction with Enhanced Ethylene and Ethanol Selectivity by Nanostructuring Polycrystalline Copper. ChemElectroChem *3*, 1012-1019.

113. Gao, Y., Wu, Q., Liang, X., Wang, Z., Zheng, Z., Wang, P., Liu, Y., Dai, Y., Whangbo, M.-H., and Huang, B. (2020). Cu_2O Nanoparticles with Both {100} and {111} Facets for Enhancing the Selectivity and Activity of CO_2 Electroreduction to Ethylene. Advanced Science *7*, 1902820.

114. Jung, H., Lee, S.Y., Lee, C.W., Cho, M.K., Won, D.H., Kim, C., Oh, H.-S., Min, B.K., and Hwang, Y.J. (2019). Electrochemical Fragmentation of Cu_2O Nanoparticles Enhancing Selective C–C Coupling from CO_2 Reduction Reaction. Journal of the American Chemical Society *141*, 4624-4633.

115. Loiudice, A., Lobaccaro, P., Kamali, E.A., Thao, T., Huang, B.H., Ager, J.W., and Buonsanti, R. (2016). Tailoring Copper Nanocrystals towards C_2 Products in Electrochemical CO_2 Reduction. Angewandte Chemie International Edition *55*, 5789-5792.

116. Suen, N.-T., Kong, Z.-R., Hsu, C.-S., Chen, H.-C., Tung, C.-W., Lu, Y.-R., Dong, C.-L., Shen, C.-C., Chung, J.-C., and Chen, H.M. (2019). Morphology Manipulation of Copper Nanocrystals and Product Selectivity in the Electrocatalytic Reduction of Carbon Dioxide. ACS Catalysis *9*, 5217-5222.

117. Zou, C., Xi, C., Wu, D., Mao, J., Liu, M., Liu, H., Dong, C., and Du, X.-W. (2019). Porous Copper Microspheres for Selective Production of Multicarbon Fuels via CO_2 Electroreduction. Small *15*, 1902582.

118. Wang, J., Cheng, T., Fenwick, A.Q., Baroud, T.N., Rosas-Hernández, A., Ko, J.H., Gan, Q., Goddard Iii, W.A., and Grubbs, R.H. (2021). Selective CO_2 Electrochemical Reduction Enabled by a Tricomponent Copolymer Modifier on a Copper Surface. Journal of the American Chemical Society *143*, 2857-2865.

119. Chen, J., Wei, X., Cai, R., Ren, J., Ju, M., Lu, X., Long, X., and Yang, S. (2022). Composition-Tuned Surface Binding on CuZn-Ni Catalysts Boosts CO_2RR Selectivity toward CO Generation. ACS Materials Letters, 497-504.

120. Ge, S., Liu, X., Liu, J., Liu, H., Liu, H., Chen, X., Wang, G., Chen, J., Zhang, G., Zhang, Y., and Li, J. (2022). Synthesis of $Ti_xSn_{1-x}O_2$ mixed metal oxide for copper catalysts as high-efficiency NH_3 selective catalytic oxidation. Fuel *314*, 123061.

121. Liang, Z.-Q., Zhuang, T.-T., Seifitokaldani, A., Li, J., Huang, C.-W., Tan, C.-S., Li, Y., De Luna, P., Dinh, C.T., Hu, Y., et al. (2018). Copper-on-nitride enhances the stable electrosynthesis of multi-carbon products from CO_2. Nature Communications *9*, 3828.

122. Chang, C.-C., Ku, M.-S., Lien, W.-H., and Hung, S.-F. (2022). Unveiling the Bonding Nature of C_3 Intermediates in the CO_2 Reduction Reaction through the Oxygen-Deficient $Cu_2O(110)$ Surface─A DFT Study. The Journal of Physical Chemistry C.

123. Pan, Y., Li, H., Xiong, J., Yu, Y., Du, H., Li, S., Wu, Z., Li, S., Lai, J., and Wang, L. (2022). Protecting the state of Cu clusters and nanoconfinement engineering over hollow mesoporous carbon spheres for electrocatalytical C-C coupling. Applied Catalysis B: Environmental *306*, 121111.

124. Ummireddi, A.K., Sharma, S.K., and Pala, R.G.S. (2022). Influence of tetraethylammonium cation on electrochemical CO_2 reduction over Cu, Ag, Ni, and Fe surfaces. Journal of Catalysis *406*, 213-221.

125. Huang, X., Kong, D., Ma, Y., Luo, B., Wang, B., and Zhi, L. (2022). An Orientated Mass Transfer in Ni-Cu Tandem Nanofibers for Highly Selective Reduction of CO_2 to Ethanol. Fundamental Research.

126. Ali, S., Razzaq, A., Kim, H., and In, S.-I. (2022). Activity, selectivity, and stability of earth-abundant $CuO/Cu_2O/Cu0$-based photocatalysts toward CO_2 reduction. Chemical Engineering Journal *429*, 131579.

127. Li, J., Kuang, Y., Meng, Y., Tian, X., Hung, W.-H., Zhang, X., Li, A., Xu, M., Zhou, W., Ku, C.-S., et al. (2020). Electroreduction of CO_2 to Formate on a Copper-Based Electrocatalyst at High Pressures with High Energy Conversion Efficiency. Journal of the American Chemical Society *142*, 7276-7282.

128. Wang, P., Qiao, M., Shao, Q., Pi, Y., Zhu, X., Li, Y., and Huang, X. (2018). Phase and structure engineering of copper tin heterostructures for efficient electrochemical carbon dioxide reduction. Nature Communications *9*, 4933.

129. Zhu, J., Wang, Y., Zhi, A., Chen, Z., Shi, L., Zhang, Z., Zhang, Y., Zhu, Y., Qiu, X., Tian, X., et al. (2022). Cation-Deficiency-Dependent CO_2 Electroreduction over Copper-Based

Ruddlesden–Popper Perovskite Oxides. Angewandte Chemie International Edition *61*, e202111670.

130. Shen, C., Wang, P., Li, L., Huang, X., and Shao, Q. (2022). Phase and structure modulating of bimetallic Cu/In nanoparticles realizes efficient electrosynthesis of syngas with wide CO/H_2 ratios. Nano Research *15*, 528-534.

131. Xia, Y., Zhang, Q., Guo, F., Wang, J., Li, W., and Xu, J. (2022). Ag@Cu with Cu–CuO interface prepared by air cold-plasma promoting the electrocatalytic reduction of CO_2 to low-carbon alcohols. Vacuum *196*, 110767.

132. Back, S., Kim, J.-H., Kim, Y.-T., and Jung, Y. (2016). Bifunctional Interface of Au and Cu for Improved CO_2 Electroreduction. ACS Applied Materials & Interfaces *8*, 23022-23027.

133. Ma, S., Sadakiyo, M., Heima, M., Luo, R., Haasch, R.T., Gold, J.I., Yamauchi, M., and Kenis, P.J.A. (2017). Electroreduction of Carbon Dioxide to Hydrocarbons Using Bimetallic Cu–Pd Catalysts with Different Mixing Patterns. Journal of the American Chemical Society *139*, 47-50.

134. Wang, J., Li, Z., Dong, C., Feng, Y., Yang, J., Liu, H., and Du, X. (2019). Silver/Copper Interface for Relay Electroreduction of Carbon Dioxide to Ethylene. ACS Applied Materials & Interfaces *11*, 2763-2767.

135. Luo, W., Xie, W., Mutschler, R., Oveisi, E., De Gregorio, G.L., Buonsanti, R., and Züttel, A. (2018). Selective and Stable Electroreduction of CO_2 to CO at the Copper/Indium Interface. ACS Catalysis *8*, 6571-6581.

136. Larrazábal, G.O., Martín, A.J., Mitchell, S., Hauert, R., and Pérez-Ramírez, J. (2016). Enhanced Reduction of CO_2 to CO over Cu–In Electrocatalysts: Catalyst Evolution Is the Key. ACS Catalysis *6*, 6265-6274.

137. Mosali, V.S.S., Zhang, X., Zhang, Y., Gengenbach, T., Guo, S.-X., Puxty, G., Horne, M.D., Bond, A.M., and Zhang, J. (2019). Electrocatalytic CO_2 Reduction to Formate on Cu Based Surface Alloys with Enhanced Selectivity. ACS Sustainable Chemistry & Engineering *7*, 19453-19462.

138. Schouten, K.J.P., Calle-Vallejo, F., and Koper, M.T.M. (2014). A Step Closer to the Electrochemical Production of Liquid Fuels. Angewandte Chemie International Edition *53*, 10858-10860.

139. Kortlever, R., Shen, J., Schouten, K.J.P., Calle-Vallejo, F., and Koper, M.T.M. (2015). Catalysts and Reaction Pathways for the Electrochemical Reduction of Carbon Dioxide. The Journal of Physical Chemistry Letters *6*, 4073-4082.

140. Adit Maark, T., and Nanda, B.R.K. (2017). Enhancing CO_2 Electroreduction by Tailoring Strain and Ligand Effects in Bimetallic Copper–Rhodium and Copper–Nickel Heterostructures. The Journal of Physical Chemistry C *121*, 4496-4504.

141. van den Berg, R., Prieto, G., Korpershoek, G., van der Wal, L.I., van Bunningen, A.J., Lægsgaard-Jørgensen, S., de Jongh, P.E., and de Jong, K.P. (2016). Structure sensitivity of Cu and CuZn catalysts relevant to industrial methanol synthesis. Nature Communications *7*, 13057.

142. Kasatkin, I., Kurr, P., Kniep, B., Trunschke, A., and Schlögl, R. (2007). Role of Lattice Strain and Defects in Copper Particles on the Activity of $Cu/ZnO/Al_2O_3$ Catalysts for Methanol Synthesis. Angewandte Chemie International Edition *46*, 7324-7327.

143. Hu, X.F., and Hirschmugl, C.J. (2005). Long-range metal-mediated interactions between S and CO on Cu(100). Physical Review B *72*, 205439.

144. Zhuang, T.-T., Liang, Z.-Q., Seifitokaldani, A., Li, Y., De Luna, P., Burdyny, T., Che, F., Meng, F., Min, Y., Quintero-Bermudez, R., et al. (2018). Steering post-C–C coupling selectivity enables high efficiency electroreduction of carbon dioxide to multi-carbon alcohols. Nature Catalysis *1*, 421-428.

145. Shao, P., Ci, S., Yi, L., Cai, P., Huang, P., Cao, C., and Wen, Z. (2017). Hollow CuS Microcube Electrocatalysts for CO_2 Reduction Reaction. ChemElectroChem *4*, 2593-2598.

146. Zhou, Y., Che, F., Liu, M., Zou, C., Liang, Z., De Luna, P., Yuan, H., Li, J., Wang, Z., Xie, H., et al. (2018). Dopant-induced electron localization drives CO_2 reduction to C_2 hydrocarbons. Nature Chemistry *10*, 974-980.

147. Tan, Z., Peng, T., Tan, X., Wang, W., Wang, X., Yang, Z., Ning, H., Zhao, Q., and Wu, M. (2020). Controllable Synthesis of Leaf-Like CuO Nanosheets for Selective CO_2 Electroreduction to Ethylene. ChemElectroChem *7*, 2020-2025.

148. Mi, Y., Peng, X., Liu, X., and Luo, J. (2018). Selective Formation of C_2 Products from Electrochemical CO_2 Reduction over $Cu_{1.8}Se$ Nanowires. ACS Applied Energy Materials *1*, 5119-5123.

149. Downes, C.A., Libretto, N.J., Harman-Ware, A.E., Happs, R.M., Ruddy, D.A., Baddour, F.G., Ferrell Iii, J.R., Habas, S.E., and Schaidle, J.A. (2020). Electrocatalytic CO_2 Reduction over Cu_3P Nanoparticles Generated via a Molecular Precursor Route. ACS Applied Energy Materials *3*, 10435-10446.

150. Zhu, Y., Yang, X., Peng, C., Priest, C., Mei, Y., and Wu, G. (2021). Carbon-Supported Single Metal Site Catalysts for Electrochemical CO_2 Reduction to CO and Beyond. Small *17*, 2005148.

151. Mohd Adli, N., Shan, W., Hwang, S., Samarakoon, W., Karakalos, S., Li, Y., Cullen, D.A., Su, D., Feng, Z., Wang, G., and Wu, G. (2021). Engineering Atomically Dispersed FeN4 Active Sites for CO_2 Electroreduction. Angewandte Chemie International Edition *60*, 1022-1032.

152. Zhang, Q., Tan, X., Bedford, N.M., Han, Z., Thomsen, L., Smith, S., Amal, R., and Lu, X. (2020). Direct insights into the role of epoxy groups on cobalt sites for acidic H_2O_2 production. Nature Communications *11*, 4181.

153. Karapinar, D., Huan, N.T., Ranjbar Sahraie, N., Li, J., Wakerley, D., Touati, N., Zanna, S., Taverna, D., Galvão Tizei, L.H., Zitolo, A., et al. (2019). Electroreduction of CO_2 on Single-Site Copper-Nitrogen-Doped Carbon Material: Selective Formation of Ethanol and Reversible Restructuration of the Metal Sites. Angewandte Chemie International Edition *58*, 15098-15103.

154. Yang, H., Wu, Y., Li, G., Lin, Q., Hu, Q., Zhang, Q., Liu, J., and He, C. (2019). Scalable Production of Efficient Single-Atom Copper Decorated Carbon Membranes for CO_2 Electroreduction to Methanol. Journal of the American Chemical Society *141*, 12717-12723.

155. Liu, G., Lee, M., Kwon, S., Zeng, G., Eichhorn, J., Buckley Aya, K., Toste, F.D., Goddard William, A., and Toma Francesca, M. (2021). CO_2 reduction on pure Cu produces only H_2 after subsurface O is depleted: Theory and experiment. Proceedings of the National Academy of Sciences *118*, e2012649118.

156. Favaro, M., Xiao, H., Cheng, T., Goddard, W.A., Yano, J., and Crumlin, E.J. (2017). Subsurface oxide plays a critical role in CO_2 activation by Cu(111) surfaces to form

chemisorbed CO_2, the first step in reduction of CO_2. Proceedings of the National Academy of Sciences *114*, 6706-6711.

157. Wuttig, A., and Surendranath, Y. (2015). Impurity ion complexation enhances carbon dioxide reduction catalysis. ACS Catal. *5*, 4479–4484.

158. Kim, D., Kley, C.S., Li, Y., and Yang, P. (2017). Copper nanoparticle ensembles for selective electroreduction of CO_2 to C_2–C_3 products. Proceedings of the National Academy of Sciences *114*, 10560.

159. Huang, J., Hörmann, N., Oveisi, E., Loiudice, A., De Gregorio, G.L., Andreussi, O., Marzari, N., and Buonsanti, R. (2018). Potential-induced nanoclustering of metallic catalysts during electrochemical CO_2 reduction. Nature communications *9*, 1-9.

160. Hodnik, N., Dehm, G., and Mayrhofer, K.J.J. (2016). Importance and Challenges of Electrochemical in Situ Liquid Cell Electron Microscopy for Energy Conversion Research. Accounts of Chemical Research *49*, 2015-2022.

161. Reske, R., Mistry, H., Behafarid, F., Roldan Cuenya, B., and Strasser, P. (2014). Particle Size Effects in the Catalytic Electroreduction of CO_2 on Cu Nanoparticles. Journal of the American Chemical Society *136*, 6978-6986.

162. Guntern, Y.T., Pankhurst, J.R., Vávra, J., Mensi, M., Mantella, V., Schouwink, P., and Buonsanti, R. (2019). Nanocrystal/metal–organic framework hybrids as electrocatalytic platforms for CO_2 conversion. Angewandte Chemie *131*, 12762-12769.

163. Zanchet, D., Micheel, C.M., Parak, W.J., Gerion, D., Williams, S.C., and Alivisatos, A.P. (2002). Electrophoretic and structural studies of DNA-directed Au nanoparticle groupings. The Journal of Physical Chemistry B *106*, 11758-11763.

164. Zhang, L., Wei, Z., Thanneeru, S., Meng, M., Kruzyk, M., Ung, G., Liu, B., and He, J. (2019). A polymer solution to prevent nanoclustering and improve the selectivity of metal nanoparticles for electrocatalytic CO_2 reduction. Angewandte Chemie *131*, 15981-15987.

165. Nguyen, V.-H., Nguyen, B.-S., Jin, Z., Shokouhimehr, M., Jang, H.W., Hu, C., Singh, P., Raizada, P., Peng, W., Shiung Lam, S., et al. (2020). Towards artificial photosynthesis: Sustainable hydrogen utilization for photocatalytic reduction of CO_2 to high-value renewable fuels. Chemical Engineering Journal *402*, 126184.

166. Romano, M.C., Anantharaman, R., Arasto, A., Ozcan, D.C., Ahn, H., Dijkstra, J.W., Carbo, M., and Boavida, D. (2013). Application of Advanced Technologies for CO_2 Capture From Industrial Sources. Energy Procedia *37*, 7176-7185.

167. Dai, Z., Deng, J., Peng, K.-J., Liu, Y.-L., and Deng, L. (2019). Pebax/PEG Grafted CNT Hybrid Membranes for Enhanced CO_2/N_2 Separation. Industrial & Engineering Chemistry Research *58*, 12226-12234.

168. Meischein, M., Garzón-Manjón, A., Frohn, T., Meyer, H., Salomon, S., Scheu, C., and Ludwig, A. (2019). Combinatorial Synthesis of Binary Nanoparticles in Ionic Liquids by Cosputtering and Mixing of Elemental Nanoparticles. ACS Combinatorial Science *21*, 743-752.

169. Sisler, J., Khan, S., Ip, A.H., Schreiber, M.W., Jaffer, S.A., Bobicki, E.R., Dinh, C.-T., and Sargent, E.H. (2021). Ethylene Electrosynthesis: A Comparative Techno-economic Analysis of Alkaline vs Membrane Electrode Assembly vs CO_2–CO–C_2H_4 Tandems. ACS Energy Letters *6*, 997-1002.

170. Pribyl-Kranewitter, B., Beard, A., Gîjiu, C.L., Dinculescu, D., and Schmidt, T.J. (2022). Influence of low-temperature electrolyser design on economic and environmental potential

of CO and HCOOH production: A techno-economic assessment. Renewable and Sustainable Energy Reviews *154*, 111807.

171. Zhu, W., Zhao, K., Liu, S., Liu, M., Peng, F., An, P., Qin, B., Zhou, H., Li, H., and He, Z. (2019). Low-overpotential selective reduction of CO_2 to ethanol on electrodeposited CuxAuy nanowire arrays. Journal of Energy Chemistry *37*, 176-182.

172. Lei, Q., Zhu, H., Song, K., Wei, N., Liu, L., Zhang, D., Yin, J., Dong, X., Yao, K., Wang, N., et al. (2020). Investigating the Origin of Enhanced C_{2+} Selectivity in Oxide-/Hydroxide-Derived Copper Electrodes during CO_2 Electroreduction. Journal of the American Chemical Society *142*, 4213-4222.

173. Zhang, B., Zhang, J., Hua, M., Wan, Q., Su, Z., Tan, X., Liu, L., Zhang, F., Chen, G., Tan, D., et al. (2020). Highly Electrocatalytic Ethylene Production from CO_2 on Nanodefective Cu Nanosheets. Journal of the American Chemical Society *142*, 13606-13613.

174. Dinh, C.-T., Burdyny, T., Kibria, M.G., Seifitokaldani, A., Gabardo, C.M., García de Arquer, F.P., Kiani, A., Edwards, J.P., De Luna, P., Bushuyev, O.S., et al. (2018). CO electroreduction to ethylene via hydroxide-mediated copper catalysis at an abrupt interface. Science *360*, 783.

175. Kim, T., and Palmore, G.T.R. (2020). A scalable method for preparing Cu electrocatalysts that convert CO_2 into C_{2+} products. Nature Communications *11*, 3622.

176. Ma, L., Hu, W., Mei, B., Liu, H., Yuan, B., Zang, J., Chen, T., Zou, L., Zou, Z., Yang, B., et al. (2020). Covalent Triazine Framework Confined Copper Catalysts for Selective Electrochemical CO_2 Reduction: Operando Diagnosis of Active Sites. ACS Catalysis *10*, 4534-4542.

177. Ren, Y., Tang, Y., Zhang, L., Liu, X., Li, L., Miao, S., Sheng Su, D., Wang, A., Li, J., and Zhang, T. (2019). Unraveling the coordination structure-performance relationship in Pt_1/Fe_2O_3 single-atom catalyst. Nature Communications *10*, 4500.

178. Choukroun, D., Daems, N., Kenis, T., Van Everbroeck, T., Hereijgers, J., Altantzis, T., Bals, S., Cool, P., and Breugelmans, T. (2020). Bifunctional Nickel–Nitrogen-Doped-Carbon-Supported Copper Electrocatalyst for CO_2 Reduction. The Journal of Physical Chemistry C *124*, 1369-1381.

Figure Captions

Figure 1. Possible mechanistic pathways of CO_2 reduction to C_1 and C_2 products on polycrystalline copper concluded from three decades' work on CO_2RR. Reproduced with permission from Nitopi et al.[32] Copyright 2019 American Chemical Society.

Figure 2. Schematic illustration for surface engineering of Cu catalysts.

Figure 3. The surface morphologies of a Cu(100) electrode with different surface treatments and reaction settings. (a-f) Each panel shows the electrode after 1 h electrolysis under different conditions; (g) Voltammetric profiles of the electropolished (EP) Cu(100) electrode (blue curve), Cu(100) with defect sites created after pulsed electrolysis (E_a = 0.6 V, E_c = −1.0 V, t_a = t_c = 1 s, red curve) and the same defective Cu(100) surface after a subsequent CO_2 electroreduction under constant potential conditions (−1.0 V, green curve); and (h) the product selectivities of the aforementioned surfaces under potentiostatic (−1.0 V) or pulsed conditions. Reproduced with permission from Arán-Ais et al.[90] Copyright 2020 Nature Publishing Group.

Figure 4. Cu-based catalysts with various morphologies and/or compositions for the CO_2RR. (a–h) EDS elemental maps of Cu foil treated under different plasma conditions. (a–d) With O_2 plasma for 20 W, 2 min; (e–f) 100 W, 2 min; and (g–h) 100 W, 2 min with H_2 plasma. Scale bars, (a–c) 300 nm; (d) 20 nm; (e–h) 200 nm. Reproduced with permission from Mistry et al.[91] Copyright 2016 Nature Publishing Group. (i–p) SEM images of the as-prepared electrodes; (i, j) TA-Cu at different magnifications; (k,l) WCO-Cu at different magnifications; (m, n) TA-Cu based GDE; and (o, p) WCO-Cu based GDE. Reproduced with permission from Zhang et al.[92] Copyright 2019 Royal Chemical Society. (q–v) SEM images of electrodeposited copper foams on a copper substrate for (q) 5 s; (r) 10 s; (s) 15 s; (t) the 30 s; (u) 60 s; and (v) nanostructure of the electrodeposited foams. Inset of (q) is a photo of a copper electrode immediately after

electrodeposition of the copper foam. Reproduced with permission from Sen et al.[93] Copyright 2014 American Chemical Society. (w–x) SEM micrographs of nanoporous copper foams electrodeposited for (w) 30 s and (x) 60 s. Reproduced with permission from Zarandi et al.[94] Copyright 2019 Elsevier.

Figure 5. Active site visualization by ReaxFF-ML. Images of the computationally produced Cu surface of (a) electro-polished, (b) after Ar plasma bombardment, and (c) predicted distribution of CO adsorption energies (ΔE_{CO}). The three dashed lines indicate the CO adsorption energies on Cu(111), (100), and (211). Reproduced with permission from Jiang et al.[95] Copyright 2020 American Chemical Society. (d) Active site visualization (ASV) of the predicted CO adsorption energies on the nanoparticle, and (e) distribution of ΔE_{CO} on the 10 nm copper nanoparticle. Reproduced with permission from Huang et al.[96] Copyright 2018 American Chemical Society.

Figure 6. Engineering Cu-surface through the regulation of various shapes. (a) TEM image of Cu spheres with an average diameter of 27 nm. Reproduced with permission from Loiudice et al.[115] Copyright 2016 John Wiley and Sons; (b) TEM images of C-Cu, and (c) H-Cu. Reproduced with permission from Suen et al.[116] Copyright 2019 American Chemical Society. (d) High-resolution TEM images OD-Cu electrode. Reproduced with permission from Li et al.[110] Copyright 2014 Nature Publishing Group. (e) TEM images of as-etched Cu NCs subjected to different periods of etching: 4 h, 8 h, 12 h, and 24 h. Reproduced with permission from Wang et al.[77] Copyright 2016 American Chemical Society. (f, h) SEM, and (g, i) HAADF-STEM of compact Cu. Reproduced with permission from Zou et al.[117] Copyright 2019 John Wiley and Sons.

Figure 7. Engineering Cu-surface through the introduction of metallic species. (a−c) Structure and phase characterization of CuSn NPs. (a) Transmission electron microscopic (TEM) image and atom model; (b) high-angle annular darkfield scanning TEM (HAADF-STEM) image; and (c)

density functional theory simulations of the CO_2 reduction reaction on Cu/SnO_2 interfaces. A free energy profile of two pathways for CO_2 electroreduction on Cu/SnO_2 interfaces. The upper and lower images are optimized geometric structures of various states (*COOH, OCHO*, and *CO) of the process on Cu/SnO_2 interfaces, respectively. H, C, O, Cu, and Sn atoms are represented by green, gray, red, reddish-brown, and dark gray spheres, respectively. Reproduced with permission from Wang et al.[128] Copyright 2018 Nature Publishing Group. (d) Ag/Cu; and (e) AgCu showing elemental distribution of Cu (red) and Ag (green); (f) Faradaic efficiencies of CO (gray), formate (blue), ethanol (violet), and ethylene (orange) for Ag/Cu catalyst in the potential range from −0.8 to −1.2 V (vs. RHE); and (g) ethylene FEs. Reproduced with permission from Wang et al.[134] Copyright 2019 American Chemical Society. (h) Bright-field TEM image of the CuIn20 sample; (i) HAADF-STEM image; and (j) the corresponding EDX elemental maps of Cu + In. Reproduced with permission from Luo et al.[135] Copyright 2018 American Chemical Society.

Figure 8. Engineering Cu-surface through insertion of non-metallic and metalloid elements. (a) Atomic models for Cu with S bonding; (b) schematic illustration of Cu_2S-Cu-V core-shell-vacancy engineering (CSVE) electrocatalyst design for production of multi-carbon alcohols from CO_2 reduction; (c) TEM; (d) EDS mapping of the original V-Cu_2S NPs, showing the uniform size and the homogeneous distribution of Cu and S; (e–f) EDS mapping; (g) high-resolution TEM; and (h) EDS line scan. Reproduced with permission from Zhuang et al.[144] Copyright 2018 Nature Publishing Group. (i) Schematic of preparing the Cu-on-Cu_3N catalyst. Reproduced with permission from Liang et al.[121] Copyright 2018 Nature Publishing Group. (j) Schematic of the wet-chemical process to synthesize Cu(B) samples. Reproduced with permission from Zhou et al.[146] Copyright 2018 Nature Publishing Group. (k) SEM images of $Cu_{1.8}Se$ NWs; (l) TEM image of the $Cu_{1.8}Se$ NWs; and (m) high-resolution TEM image and element mapping of $Cu_{1.8}Se$ NWs.

Reproduced with permission from Mi et al.[148] Copyright 2018 American Chemical Society. (n) TEM image of the Cu_3P NPs; (o) HRTEM image with outlined region used for fast Fourier transform (FFT) analysis; and (p) FFT pattern indexed to the [0001] zone axis. Reproduced with permission from Downes et al.[149] Copyright 2020 American Chemical Society.

Figure 9. Engineering Cu-surface through the construction of single Cu sites. (a) HAADF-STEM images and enlarged images; (b-e) EDS images of Cu-SA/NPC by HAADF-STEM; and (f) free energy diagrams calculated at a potential of −0.36 V for CO_2 reduction to CH_3COCH_3 on Cu-pyridinic-N_4 and Cu-pyrrolic-N_4 sites of Cu-SA/NPC. Reproduced with permission from Zhang et al.[152] Copyright 2020 Nature Publishing Group. (g) Cu K-edge EXAFS analysis in the Fourier-transformed space; (h) HAADF-STEM image of $Cu_{0.5}NC$. Reproduced with permission from Karapinar et al.[153] Copyright 2019 John Wiley and Sons. (i) HAADF-STEM images of CuSAs/TCNFs; (j) the white dot is an isolated copper atom; (k) FT at R space of three samples; (l) fitting for EXAFS data of CuSAs/TCNFs; (m) optimized atomic structures of CuSAs/TCNFs and proposed reaction paths for CO_2 electroreduction; (n-o) free energy diagram of CO_2 to CO on pyridine N, Ni-N_4, and Cu-N_4 structure; (p) illustration of CO_2 diffusion on two samples; and (q) free energies for conversion of *CO to CH_3OH on Cu-N_4 structure. Reproduced with permission from Yang et al.[154] Copyright 2019 American Chemical Society.

Figure 10. Investigation of various Cu surfaces using APXPS. (a) LEED pattern obtained at an electron kinetic energy of 110 eV and SEM micrograph of the Cu surface after sputtering and annealing cycles obtained by detecting the secondary electrons (SE) with a kinetic energy of the primary beam of 5 keV; (b) Schematic of the APXPS measurements with the highlighted probed volume (3λ) along the (111) direction; (c-d) C 1s and O 1s photoelectron peaks and multipeak fitting results were obtained for the various experimental conditions and investigated surfaces (at

298 K). Predicted structures for 1/4 ML of physisorbed *l*-CO_2 on various Cu surfaces (Cu, light blue; C, brown; O, red, but Osub is marked in orange); top and side views of (e) pristine Cu(111), ΔG = +0.27 eV, *p*thresh = 33 atm; (f) Cu(111) with 1/4 ML O_{ads}; (g) Cu(111) with 1/4 ML O_{sub}; and (h) Cu(111) with 1/4 ML of both O_{ads} and O_{sub}; top and side views with chemical illustration of predicted structures (i) on pristine Cu(111), ΔG = +1.07 eV; (j) on Cu(111) with 1/4 ML O_{sub}, ΔG = -0.06 eV; and (k) on Cu(111) with 1/2 ML O_{sub}, ΔG = +0.28 eV. Reproduced with permission from Favaro et al.[156] Copyright 2017 National Acad Sciences.

Figure 11. Summary of nanoscale degradation mechanism of Cu-based nanostructures during CO_2RR process. Reproduced with permission from Popović et al.[82] Copyright 2020 John Wiley and Sons.

Table 1. Cu-based electrocatalysts for the CO_2RR to hydrocarbons.

Table 1.

Sr.No	Electrocatalysts	Electrolyte	C_2 and C_3 Product/FE %	Ref.
1	cube-shaped copper	0.1 M $KHCO_3$	C_2H_4 (41%)	[115]
2	Cu-SA/NPC	0.1M $KHCO_3$	acetone (36.7%)	[152]
3	4H/fcc Au@Cu	0.1 M $KHCO_3$	C_2H_4 (44.9%)	[53]
4	CuO/NG_AN	0.1 M $KHCO_3$	C_2H_4 (29%)	[147]
5	Cu_3N	0.1 M $KHCO_3$	C_2H_4 (60%)	[147]
6	Cu_2O	0.1 M $KHCO_3$	C_2H_4 (57.3%)	[114]
7	Cu_3N	0.1 M $KHCO_3$	EtOH (8%) C_2H_6 (12%) C_2H_4 (66%)	[171]
8	PAN-Cu (containing Cu, and $Cu(OH)_2$)	0.1 M $KHCO_3$	C_2H_4 (76.73%)	[172]
9	Cu nanowires	0.1 M $KHCO_3$	EtOH (50%)	[81]
10	concave octahedral Cu_2O	0.1 M $KHCO_3$	C_{2+} (48.3%)	[108]
11	Nanodefective Cu Nanosheets	0.1 M $KHCO_3$	C_2H_4 (83.2%)	[173]
13	Cu_xAu_y NWAs	0.1 M $KHCO_3$	EtOH (48%)	[171]
14	anodized copper (ANCu) $Cu(OH)_2$	0.1 M $KHCO_3$	C_2H_4 (~40%)	[27]
15	Cu_xO nanowires grown on Cu gauzes	0.1 M $KHCO_3$	C_2H_4 (~ 30%)	[92]
16	Cu_2O and defects on Cu(100)	0.1 M $KHCO_3$	C_2H_4 (45%)	[90]
17	copper electrocatalyst	10 M KOH	C_2H_4 (70%)	[174]
18	Cu foils with Cu_KBr (60 s)	0.1 M KBr	C_2H_4 (50.9%)	[175]
19	cubes with 44 nm edge length	0.1 M $KHCO_3$	C_2H_4 (41%)	[115]
20	CTF-Cu-4.8%	0.3 M KCl solution	C_2H_4 (35.0%) acetate (33.4%)	[176]
21	Cu nanowires (NWs) with Cu(100)	0.1 M $KHCO_3$	C_2H_4 (35%)	[177]
22	plasma-activated Cu foils	0.1 M $KHCO_3$	C_2H_4 (60%)	[91]
23	Cu foil with Cu (I) oxide surface	0.05 m $KHCO_3$	C_2H_4 (56%)	[67]

24	Cu−Ni−N−AC	0.1 M $KHCO_3$	C_2H_4 (30.7%)	[178]
25	truncated-octahedral Cu_2O (t-Cu_2O)	0.1 M $KHCO_3$	C_2H_4 (59%)	[113]

Figure 1.

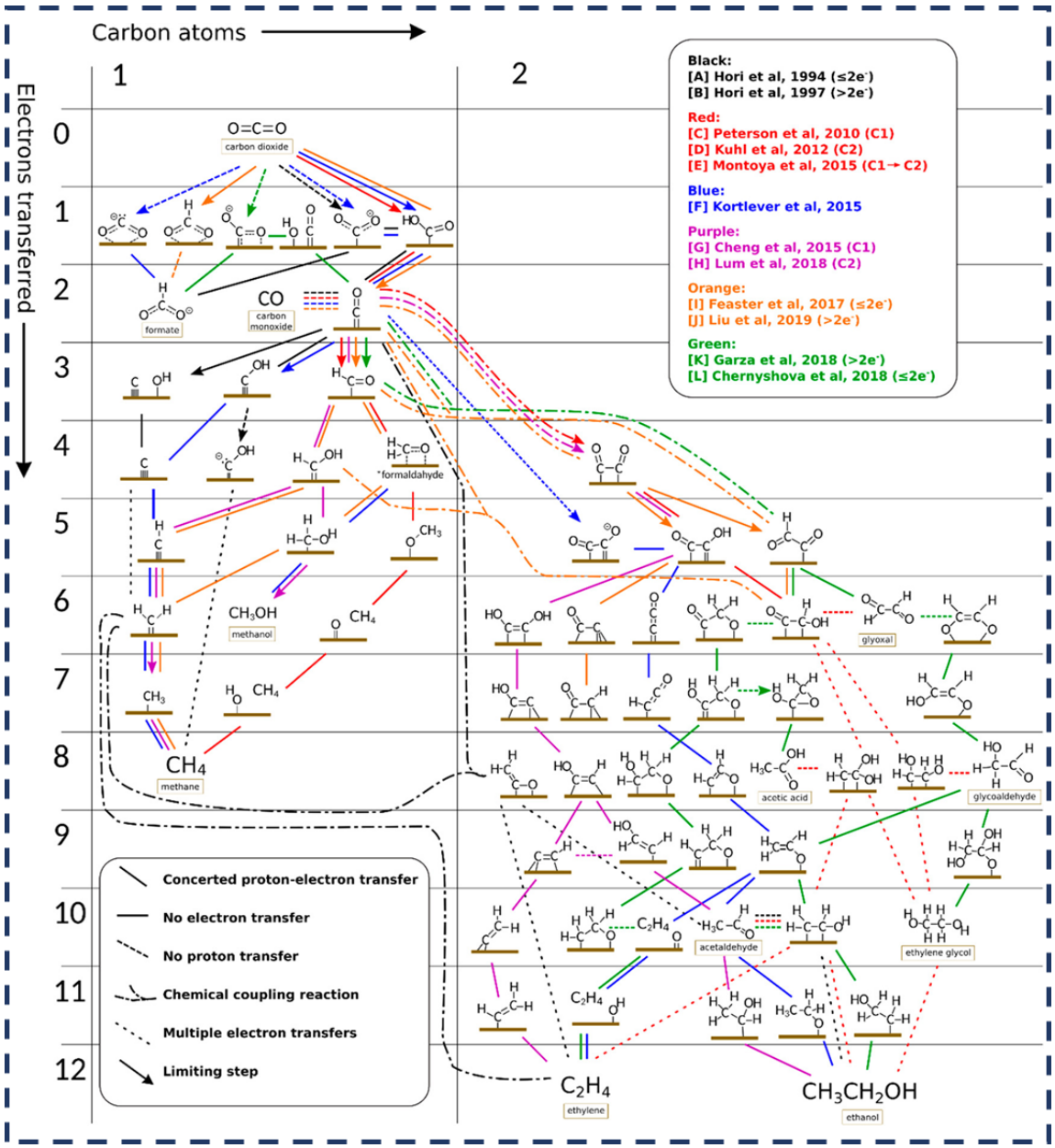
Carbon atoms
1
2
Electrons transferred
0
1
2
3
4
5
6
7
8
9
10
11
12
Black:
[A] Hori et al, 1994 (≤2e⁻)
[B] Hori et al, 1997 (>2e⁻)
Red:
[C] Peterson et al, 2010 (C1)
[D] Kuhl et al, 2012 (C2)
[E] Montoya et al, 2015 (C1→C2)
Blue:
[F] Kortlever et al, 2015
Purple:
[G] Cheng et al, 2015 (C1)
[H] Lum et al, 2018 (C2)
Orange:
[I] Feaster et al, 2017 (≤2e⁻)
[J] Liu et al, 2019 (>2e⁻)
Green:
[K] Garza et al, 2018 (>2e⁻)
[L] Chernyshova et al, 2018 (≤2e⁻)
O=C=O
carbon dioxide
formate
CO
carbon monoxide
*formaldahyde
CH3OH
methanol
CH4
methane
glyoxal
acetic acid
glycoaldehyde
acetaldehyde
ethylene glycol
C2H4
ethylene
CH3CH2OH
ethanol
Concerted proton-electron transfer
No electron transfer
No proton transfer
Chemical coupling reaction
Multiple electron transfers
Limiting step

Figure 2.

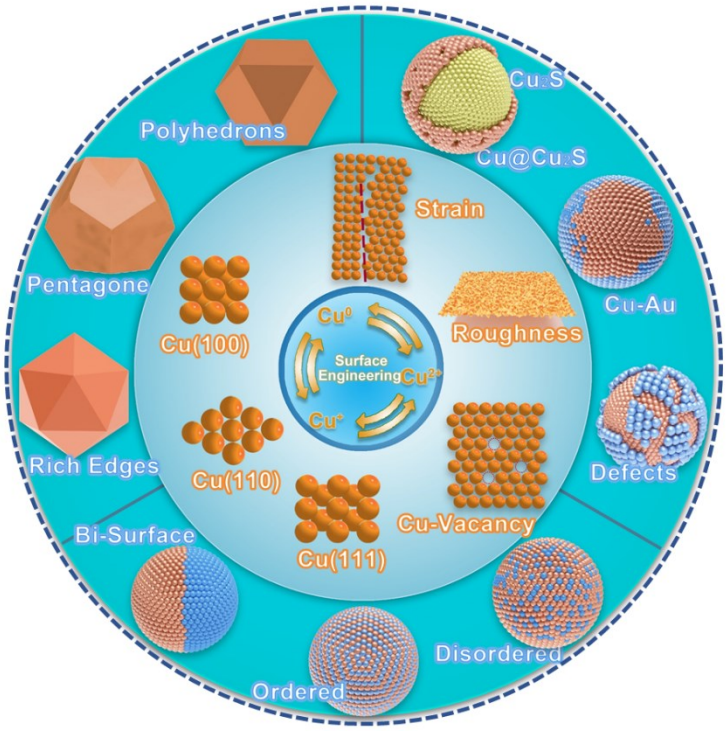
Polyhedrons
Cu2S
Cu@Cu2S
Strain
Pentagone
Cu-Au
Cu(100)
Roughness
Cu0
Surface Engineering
Cu2+
Cu+
Rich Edges
Defects
Cu(110)
Bi-Surface
Cu-Vacancy
Cu(111)
Disordered
Ordered

Figure 3.

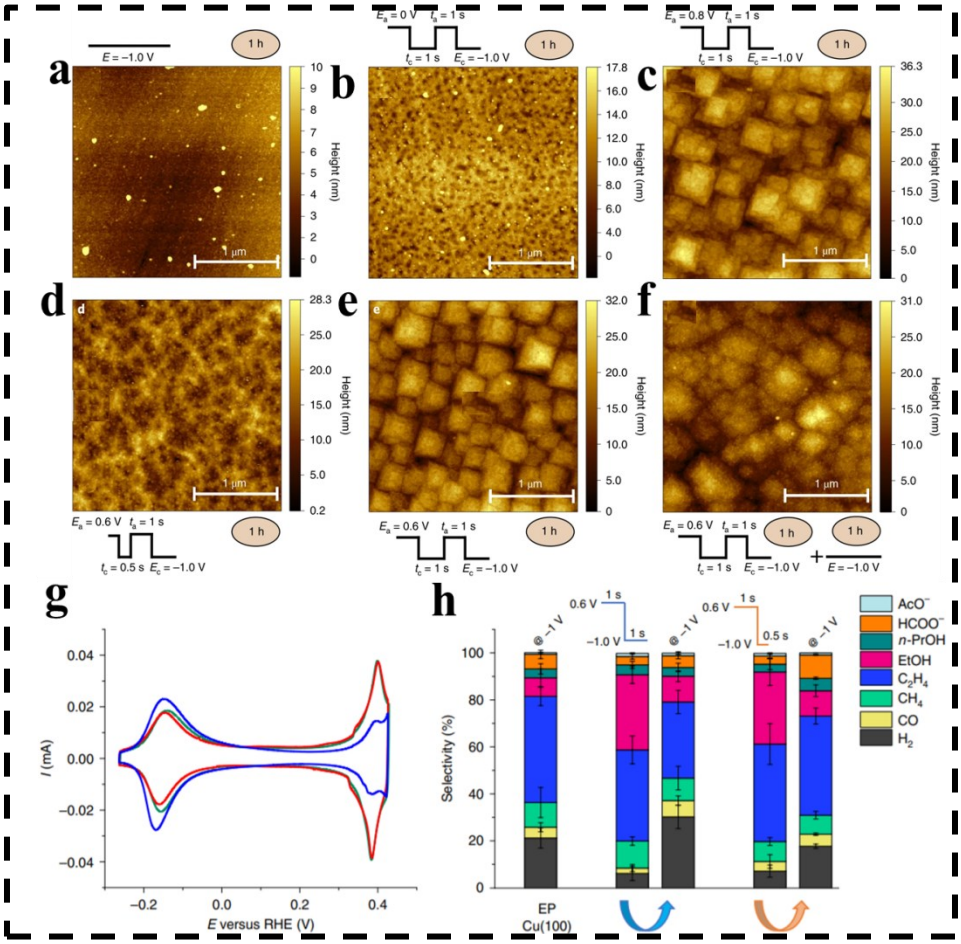
a
b
c
d
e
f
g
h
E = −1.0 V
1 h
1 μm
Height (nm)
E versus RHE (V)
I (mA)
Selectivity (%)
EP
Cu(100)
AcO⁻
HCOO⁻
n-PrOH
EtOH
C2H4
CH4
CO
H2

Figure 4.

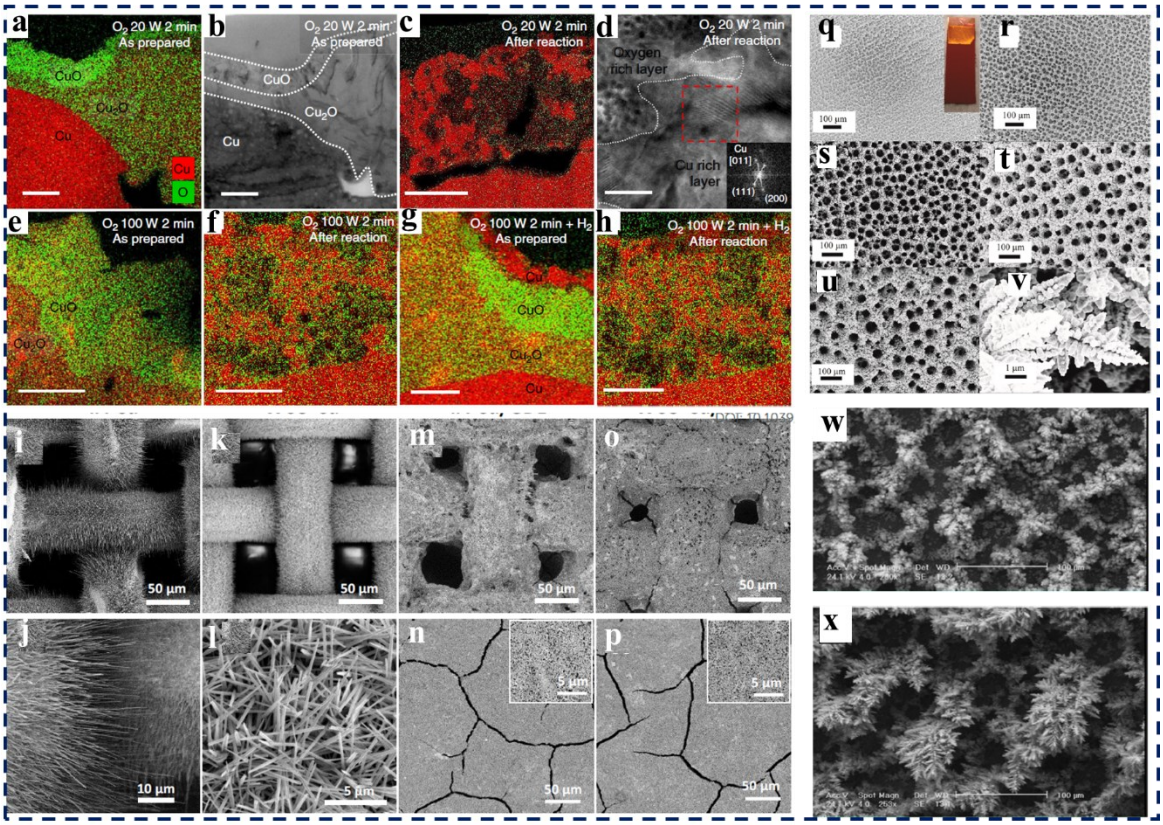
a
O2 20 W 2 min
As prepared
CuO
Cu2O
Cu
Cu
O
b
O2 20 W 2 min
As prepared
CuO
Cu2O
Cu
c
O2 20 W 2 min
After reaction
d
O2 20 W 2 min
After reaction
Oxygen rich layer
Cu rich layer
Cu
[011]
(111)
(200)
e
O2 100 W 2 min
As prepared
CuO
Cu2O
f
O2 100 W 2 min
After reaction
g
O2 100 W 2 min + H2
As prepared
Cu
CuO
Cu2O
Cu
h
O2 100 W 2 min + H2
After reaction
i
50 µm
k
50 µm
m
50 µm
o
50 µm
j
10 µm
l
5 µm
n
5 µm
50 µm
p
5 µm
50 µm
q
100 µm
r
100 µm
s
100 µm
t
100 µm
u
100 µm
v
1 µm
w
x

Figure 5.

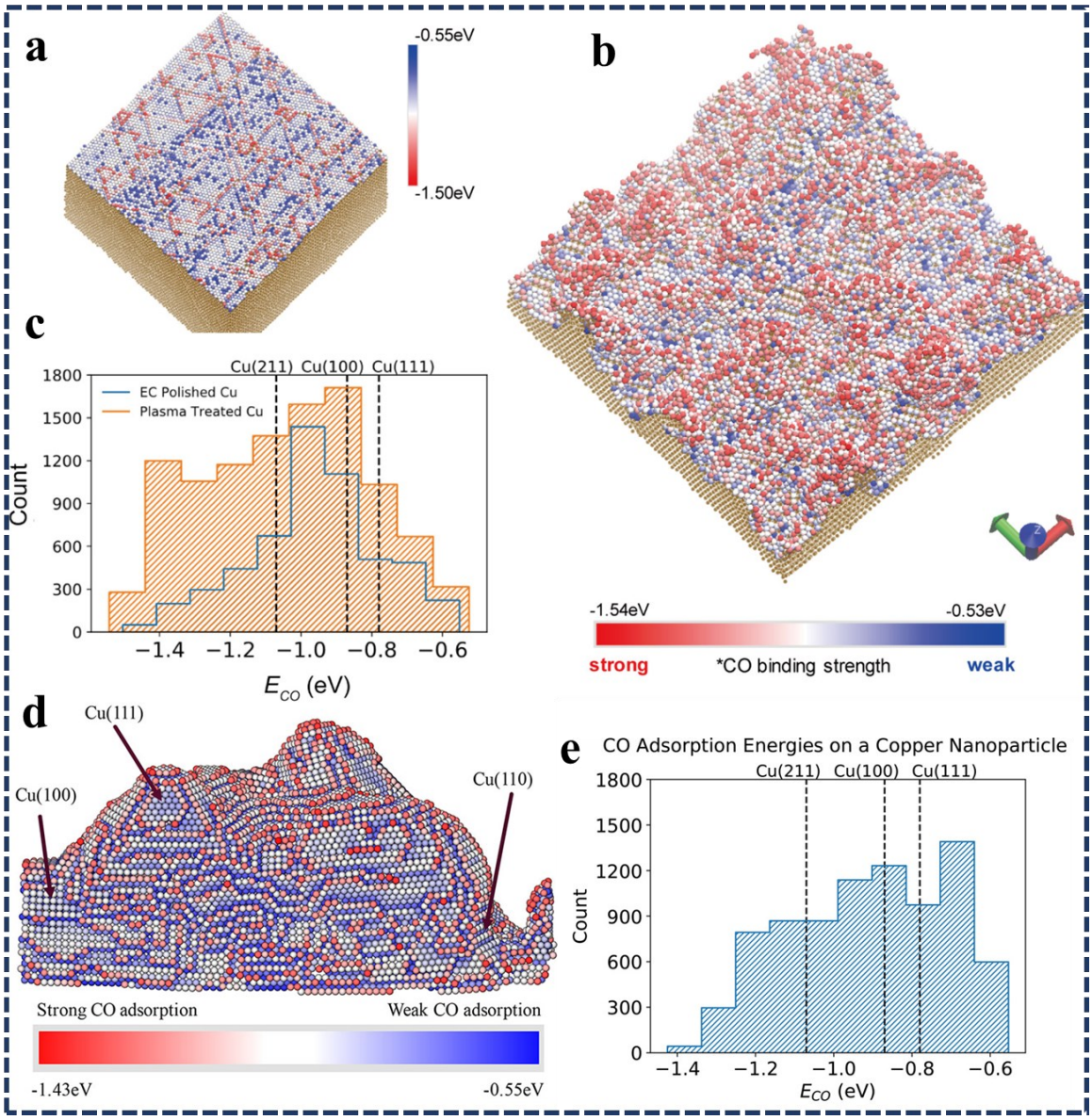
a
-0.55eV
-1.50eV
b
-1.54eV
-0.53eV
strong
*CO binding strength
weak
c
Cu(211) Cu(100) Cu(111)
EC Polished Cu
Plasma Treated Cu
Count
E_{CO} (eV)
d
Cu(111)
Cu(100)
Cu(110)
Strong CO adsorption
Weak CO adsorption
-1.43eV
-0.55eV
e
CO Adsorption Energies on a Copper Nanoparticle
Cu(211) Cu(100) Cu(111)
Count
E_{CO} (eV)

Figure 6.

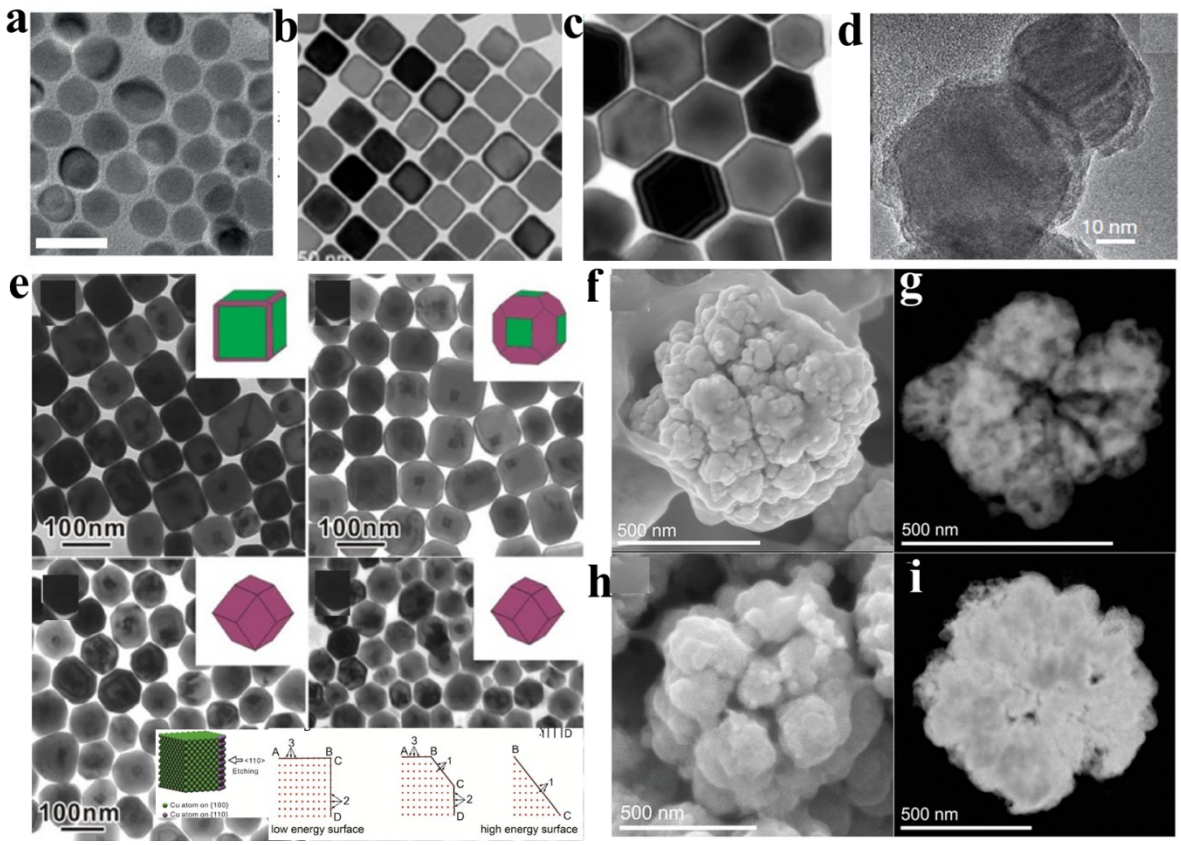
a
b
c
d
10 nm
e
100nm
100nm
100nm
f
500 nm
g
500 nm
h
500 nm
i
500 nm
low energy surface
high energy surface

Figure 7.

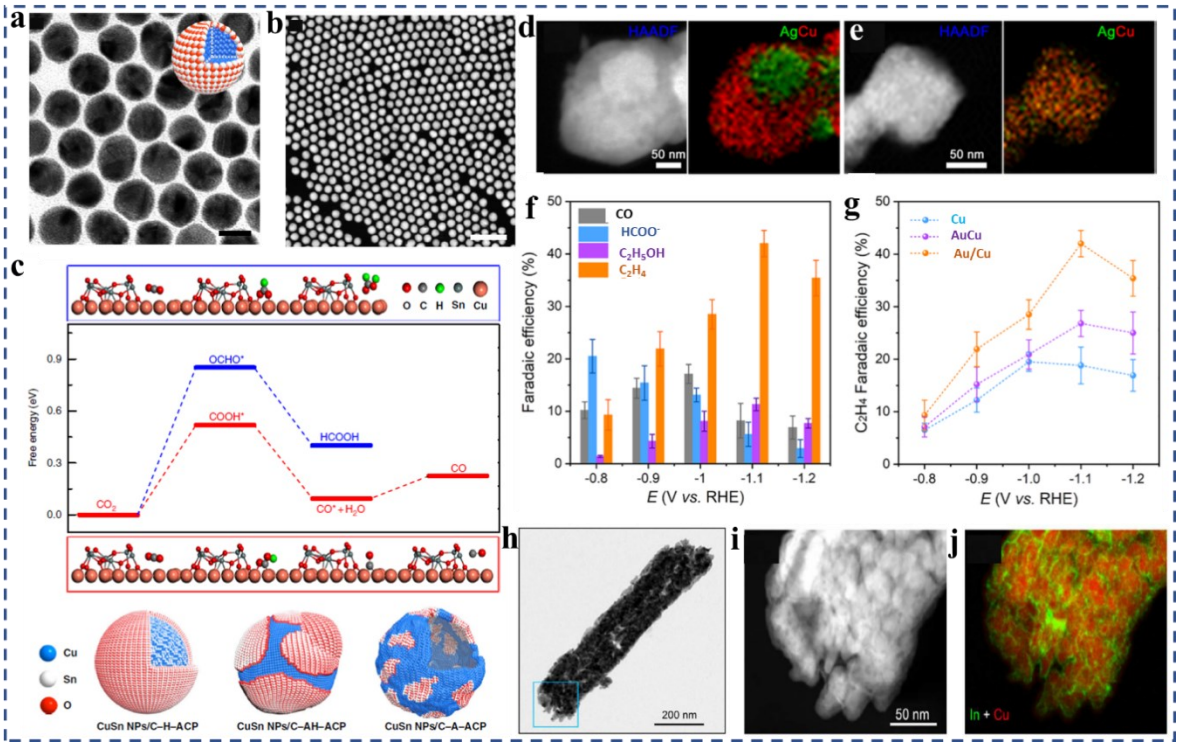
a
b
d
HAADF
AgCu
50 nm
e
HAADF
AgCu
50 nm
c
O C H Sn Cu
OCHO*
COOH*
HCOOH
CO
CO2
CO* + H2O
Free energy (eV)
Cu
Sn
O
CuSn NPs/C–H–ACP
CuSn NPs/C–AH–ACP
CuSn NPs/C–A–ACP
f
CO
HCOO-
C2H5OH
C2H4
Faradaic efficiency (%)
E (V vs. RHE)
g
Cu
AuCu
Au/Cu
C2H4 Faradaic efficiency (%)
E (V vs. RHE)
h
200 nm
i
50 nm
j
In + Cu

Figure 8.

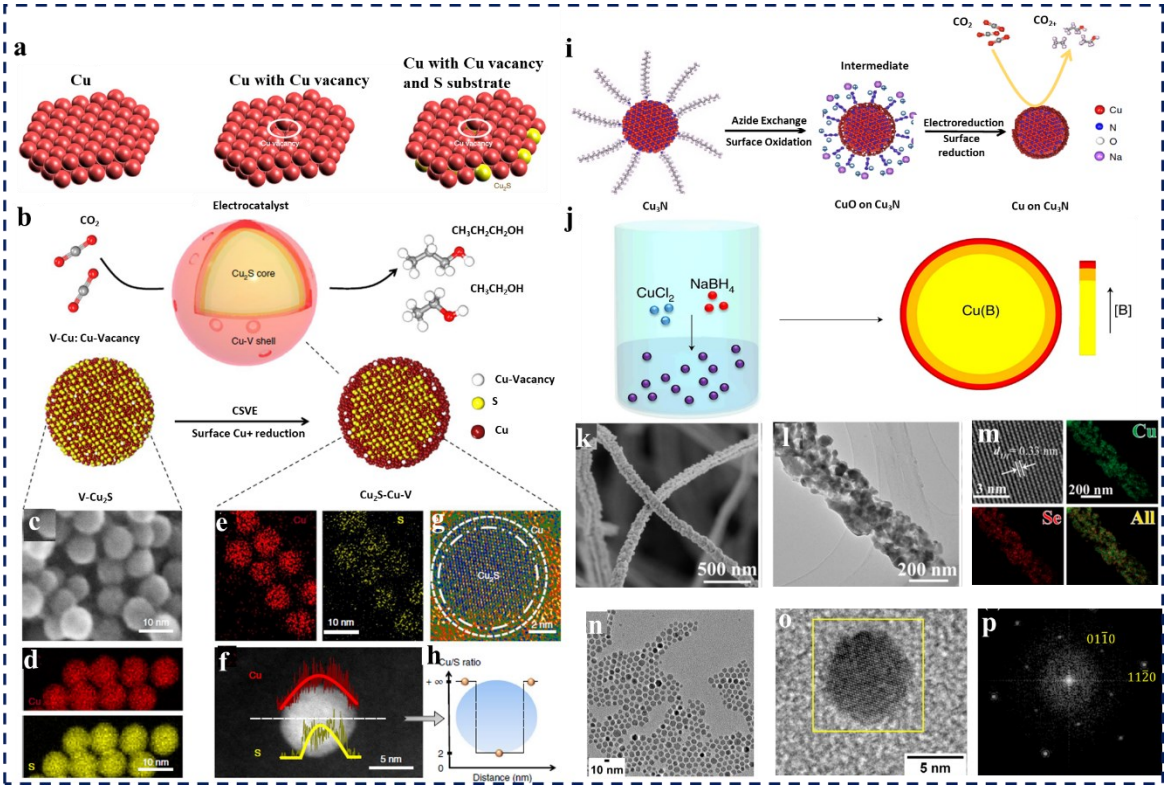
a
Cu
Cu with Cu vacancy
Cu with Cu vacancy and S substrate
b
Electrocatalyst
CO2
Cu2S core
Cu-V shell
CH3CH2CH2OH
CH3CH2OH
V-Cu: Cu-Vacancy
CSVE
Surface Cu+ reduction
Cu-Vacancy
S
Cu
V-Cu2S
Cu2S-Cu-V
c
d
e
f
g
h
Cu/S ratio
Distance (nm)
i
Cu3N
Azide Exchange
Surface Oxidation
Intermediate
CuO on Cu3N
Electroreduction
Surface reduction
Cu on Cu3N
Cu
N
O
Na
j
CuCl2
NaBH4
Cu(B)
[B]
k
500 nm
l
200 nm
m
0.33 nm
3 nm
Cu
200 nm
Se
All
n
10 nm
o
5 nm
p
01$\bar{1}$0
11$\bar{2}$0

Figure 9.

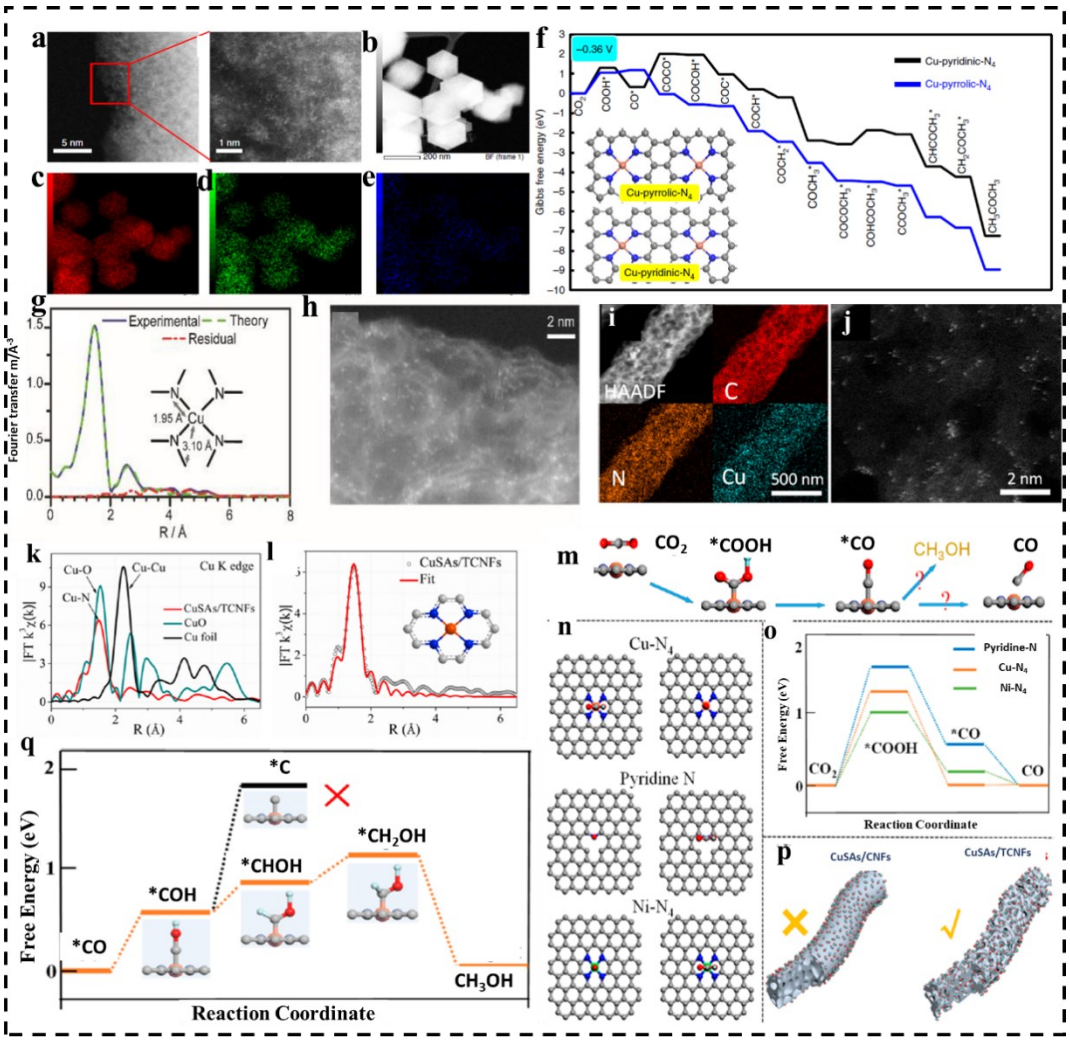
a
5 nm
1 nm
b
200 nm
BF (frame 1)
c
d
e
f
−0.36 V
Cu-pyridinic-N4
Cu-pyrrolic-N4
Gibbs free energy (eV)
Cu-pyrrolic-N4
Cu-pyridinic-N4
g
Experimental
Theory
Residual
Fourier transfer m/Å⁻³
1.95 Å
Cu
3.10 Å
R / Å
h
2 nm
i
HAADF
C
N
Cu
500 nm
j
2 nm
k
Cu-O
Cu-Cu
Cu K edge
Cu-N
CuSAs/TCNFs
CuO
Cu foil
|FT k³χ(k)|
R (Å)
l
CuSAs/TCNFs
Fit
|FT k³χ(k)|
R (Å)
m
CO2
*COOH
*CO
CH3OH
CO
n
Cu-N4
Pyridine N
Ni-N4
o
Pyridine-N
Cu-N4
Ni-N4
Free Energy (eV)
CO2
*COOH
*CO
CO
Reaction Coordinate
p
CuSAs/CNFs
CuSAs/TCNFs
q
*C
*CH2OH
*CHOH
*COH
*CO
CH3OH
Free Energy (eV)
Reaction Coordinate

Figure 10.

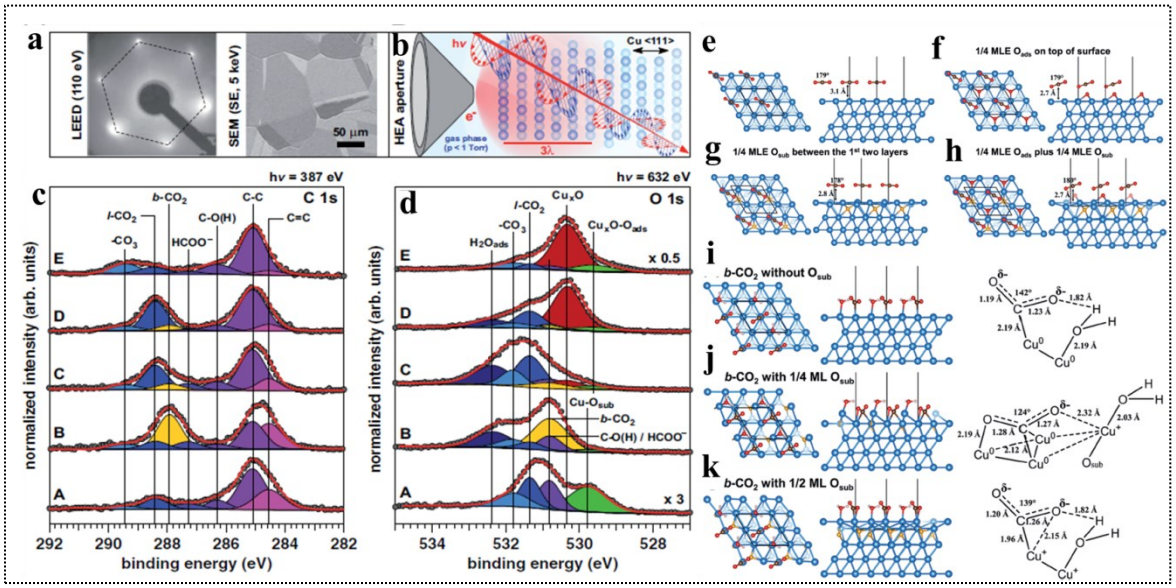
a
LEED (110 eV)
SEM (SE, 5 keV)
50 µm
b
HEA aperture
hν
e⁻
gas phase
(p < 1 Torr)
Cu <111>
3λ
c
hν = 387 eV
C 1s
b-CO2
C-C
l-CO2
C-O(H)
C=C
-CO3
HCOO⁻
E
D
C
B
A
normalized intensity (arb. units)
292
290
288
286
284
282
binding energy (eV)
d
hν = 632 eV
O 1s
CuxO
l-CO2
-CO3
H2Oads
CuxO-Oads
x 0.5
Cu-Osub
b-CO2
C-O(H) / HCOO⁻
x 3
534
532
530
528
binding energy (eV)
e
f
1/4 MLE Oads on top of surface
g
1/4 MLE Osub between the 1st two layers
h
1/4 MLE Oads plus 1/4 MLE Osub
i
b-CO2 without Osub
j
b-CO2 with 1/4 ML Osub
k
b-CO2 with 1/2 ML Osub

Figure 11.

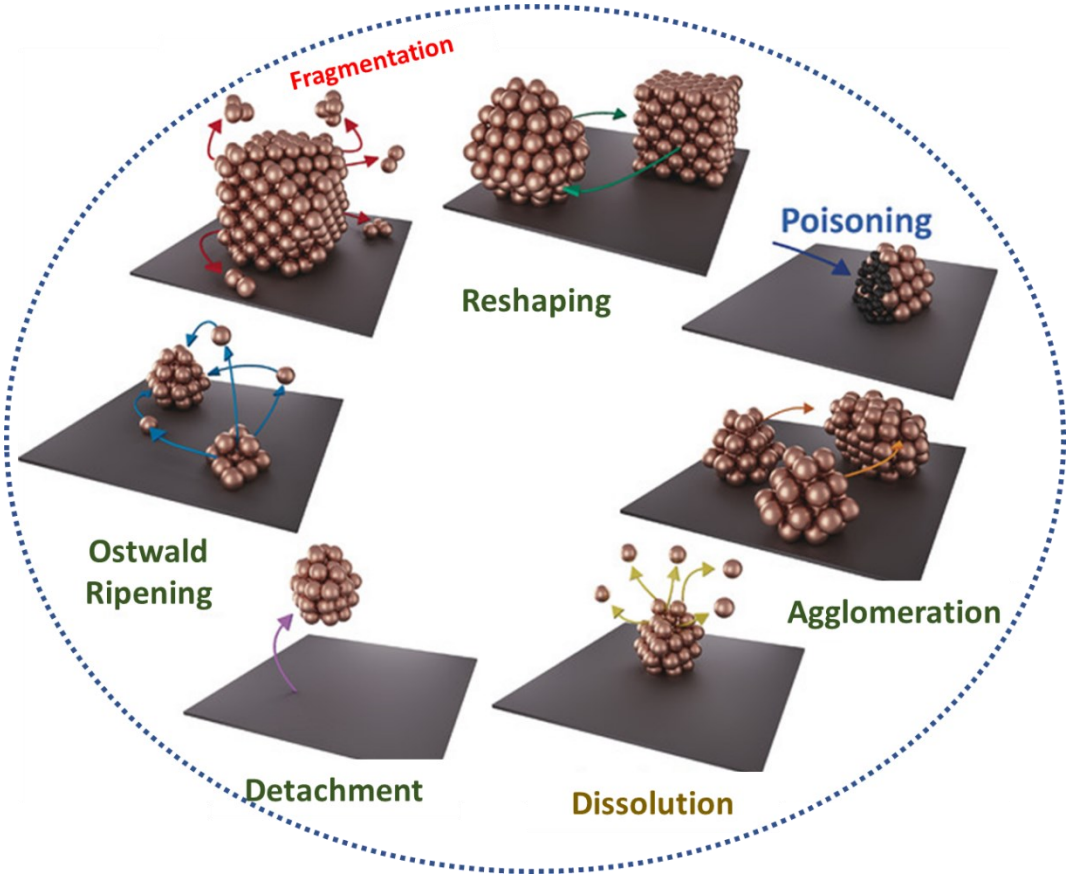
Fragmentation
Reshaping
Poisoning
Ostwald
Ripening
Agglomeration
Detachment
Dissolution